

# The transition from the adiabatic to the sudden limit in core level photoemission: A model study of a localized system

J.D. Lee and O. Gunnarsson  
*Max-Planck Institut für Festkörperforschung,  
 Heisenbergstrasse 1, D-70569 Stuttgart, Germany*

L. Hedin  
*Department of Theoretical Physics, University of Lund,  
 Sölvegatan 14 A, S-223 62 Lund, Sweden*  
 (April 6, 2018)

We consider core electron photoemission in a localized system, where there is a charge transfer excitation. Examples are transition metal and rare earth compounds, chemisorption systems, and high  $T_c$  compounds. The system is modelled by three electron levels, one core level and two outer levels. In the initial state the core level and one outer level is filled (a spinless two-electron problem). This model system is embedded in a solid state environment, and the implications of our model system results for solid state photoemission are discussed. When the core hole is created, the more localized outer level (d) is pulled below the less localized level (L). The spectrum has a leading peak corresponding to a charge transfer between L and d ("shake-down"), and a satellite corresponding to no charge transfer. The model has a Coulomb interaction between these levels and the continuum states into which the core electron is emitted. The model is simple enough to allow an exact numerical solution, and with a separable potential an analytic solution. Analytic results are also obtained in lowest order perturbation theory, and in the high energy limit of the semiclassical approximation. We calculate the ratio  $r(\omega)$  between the weights of the satellite and the main peak as a function of the photon energy  $\omega$ . The transition from the adiabatic to the sudden limit is found to take place for quite small kinetic energies of the photoelectron. For such small energies, the variation of the dipole matrix elements is substantial and described by the energy scale  $\tilde{E}_d$ . Without the coupling to the photoelectron, the corresponding ratio  $r_0(\omega)$  shows a smooth turn-on of the satellite intensity, due to the turn on of the dipole matrix element. The characteristic energy scales are  $\tilde{E}_d$  and the satellite excitation energy  $\delta E$ . When the interaction potential with the continuum states is introduced a new energy scale  $\tilde{E}_s = 1/(2\tilde{R}_s^2)$  enters, where  $\tilde{R}_s$  is a length scale of the interaction (scattering) potential. At threshold there is typically a (weak) *constructive* interference between intrinsic and extrinsic contributions, and the ratio  $r(\omega)/r_0(\omega)$  is larger than its limiting value for large  $\omega$ . The interference becomes small or weakly destructive for photoelectron energies of the order  $\tilde{E}_s$ . For larger photoelectron energies  $r(\omega)/r_0(\omega)$  therefore typically has a weak undershoot. If this undershoot is neglected,  $r(\omega)/r_0(\omega)$  reaches its limiting value on the energy scale  $\tilde{E}_s$  for the parameter range considered here. In a "shake-up" scenario, where the two outer levels do not cross as the core hole is created, we instead find that  $r(\omega)/r_0(\omega)$  is typically reduced for small  $\omega$  by interference effects, as in the case of plasmon excitation. For the "shake-down" case, however, the results are very different from those for a simple metal, where plasmons dominate the picture. In particular, the adiabatic to sudden transition takes place at much lower energies in the case of a localized excitation. The reasons for the differences are briefly discussed.

## I. INTRODUCTION

X-ray photoemission spectroscopy PES is a useful tool for studying the electronic structure of solids. The theoretical description of PES is however very complicated<sup>1,2</sup> and almost all work has been based on the so-called sudden approximation.<sup>3,4</sup> The photoemission spectrum is then described by the electron spectral function convoluted by a loss function, describing the transport of the emitted electron to the surface. The sudden approximation becomes exact in the limit when the kinetic energy of the emitted electron becomes infinite.<sup>3,4</sup> In this limit

we can distinguish between intrinsic satellites, appearing in the electron spectral function, and extrinsic satellites, appearing in the loss function. For lower kinetic energy, this distinction is blurred due to interference effects, and the satellite weights are expected to be quite different as we approach the opposite limit, the adiabatic limit, of low kinetic energy.<sup>3</sup> It is then interesting to ask at what kinetic energy the sudden approximation becomes accurate. This issue has been studied extensively for the case when the emitted electron couples to plasmons, and it has been found that the sudden approximation becomes valid only for very large ( $\sim$  keV) kinetic energies.<sup>4-6</sup>

A semi-classical approach has been found to work ex-

ceedingly well for the study of plasmon satellites.<sup>4,5</sup> In such a picture, one may take the emitted electron to move as a classical particle away from the region where the hole was created. The system then sees the potential from both the created electron and hole. Initially the electron potential cancels the hole potential, but as the electron moves away, the hole potential is gradually switched on. The switching-on of the hole potential may lead to the creation of excitations. If the kinetic energy of the electron is sufficiently large, we can consider the hole potential as being switched on instantly, and the creation of excitations around the hole then reaches a limiting value, the sudden limit. In the semi-classical picture, the perturbation is turned on during a time  $\tau = R_0/v$ , where  $v$  is the photoelectron velocity and  $R_0$  is the range of the interaction (scattering) potential between the emitted electron and the excitations. In this picture we also need to determine the relevant time scale  $\tau_{\max}$  so that the sudden limit is reached if  $\tau \ll \tau_{\max}$  or  $v \gg R_0/\tau_{\max}$ . Our analysis within the semi-classical framework shows that  $1/\tau_{\max}$  is related to the energy  $\delta E$  of the relevant excitation of the system and to the strength  $\tilde{V}$  of the scattering potential.

We find a different characteristic energy scale  $\tilde{E}_s = 1/(2\tilde{R}_s^2)$ , where  $\tilde{R}_s$  is a characteristic length scale of the scattering potential. On dimensional grounds one may argue that the adiabatic-sudden approximation takes place when the kinetic energy of the emitted electron is comparable to  $\tilde{E}_s$ . This would differ dramatically from the semi-classical approach, where the transition takes place for energy of the order  $1/(\tilde{E}_s\tau_{\max}^2)$ , i.e. e.g.,  $(\delta E)^2/\tilde{E}_s$  or  $\tilde{V}^2/\tilde{E}_s$ . Alternatively, and again on dimensional grounds, one may argue that the sudden approximation becomes valid when the kinetic energy of the emitted electron is much larger than the energy  $\delta E$  of the relevant excitations of the system,<sup>7</sup> in strong contrast to the two criteria above. This latter criterion is however not true in general.<sup>8</sup>

For many systems with strong correlations, the core level spectrum can be understood in a charge transfer scenario.<sup>9</sup> This is illustrated in Fig. 1 for a Cu compound, e.g., a Cu halide. In the ground-state, Cu has essentially the configuration  $d^9$  and all the ligand orbitals are filled. In the presence of a Cu core hole, it becomes energetically favorable to transfer an electron from a ligand to the d-shell, obtaining a  $d^{10}$  configuration on the Cu atom with the core hole. Due to the hybridization between the  $d^9$  and  $d^{10}$  configurations, the states are actually mixtures of the two configurations, as indicated in Fig. 1. In the photoemission process there is a nonzero probability that the outer electron will not stay on the ligand, but is transferred to the lower energy  $d$ -like state. This “shake-down” process corresponds to the leading peak in the spectrum, while the process where the outer electron stays on the ligand corresponds to the satellite. This kind of model has been applied to rare earth compounds,<sup>9,10</sup> chemisorption systems,<sup>11,12</sup> transi-

tion metal compounds,<sup>13–17</sup> and High  $T_c$  compounds.<sup>18</sup>

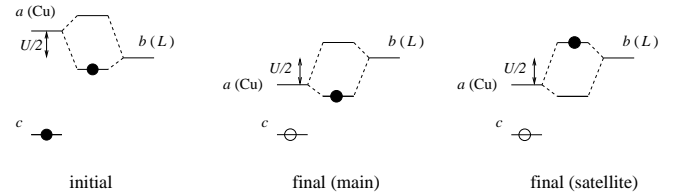


FIG. 1. Schematic view of the Cu 3s charge transfer photoemission. Here  $a$  is the Cu 3d level and  $b$  is a ligand (L) valence state for the symmetric case.

Our simple model allows an accurate numerical calculation of the photocurrent either by integrating the time-dependent Schrödinger equation or by directly inverting a resolvent operator (QM). We also derive analytic results with a separable potential. These results are compared with the semi-classical theory (SC), and with first order perturbation theory (PT). In both these cases we have analytic results, which is very useful for understanding the physics of the problem.

The impurity model discussed here differs in certain important aspects from a real solid. To start with, for a solid we never reach the limit of a pure intrinsic spectrum since when the cross section for extrinsic scattering goes to zero, the range from which the photoelectrons come goes to infinity. In our impurity model, on the other hand, the extrinsic scattering approaches zero at high kinetic energies. Secondly, for a solid, we discuss excitations in the continuum and not as here discrete energy levels.

For the coupling to plasmons, the adiabatic-sudden transition takes place at large kinetic energies where the SC approximation is very accurate.<sup>4,5</sup> The relevant length scale is given by the plasmon wave length  $\lambda = 2\pi/q$  and the relevant time by the inverse plasmon frequency  $\omega_q$ . Large interference effects are then connected with a large phase velocity  $\omega_q/q$ , as discussed e.g. by Inglesfield.<sup>19</sup> Since long wave-length plasmons play an important role these large interference effects for small  $q$  delay the approach to the sudden limit, which only is reached at very high kinetic energies ( $\sim$  keV).

For the localized excitations studied here the relevant length scale is much shorter. The SC theory then predicts that the transition takes place at correspondingly smaller kinetic energies. This is indeed what we find from the exact solution of our model. This has two consequences. Firstly, the SC treatment itself is not valid at such small energies, and we have to rely on QM treatments. Actually, although the SC treatment correctly predicts a small transition energy, we find it predicts qualitatively wrong dependencies on the relevant parameters. Secondly, the smaller energy scale means that the energy variation of the dipole matrix elements becomes very important. The

dipole matrix element grows rapidly on an energy scale  $\tilde{E}_d$ , which can become very important for the adiabatic-sudden transition.

We study the ratio  $r(\omega)$  between the weights of the satellite and the main peak as a function of the photon energy  $\omega$  for the emission from a  $3s$  level. First we consider the case when the scattering potential between the electron and the target is neglected. We find that the corresponding ratio  $r_0(\omega)$  strongly depends on the ratio between the excitation energy  $\delta E$  and  $\tilde{E}_d$ . If  $\delta E/\tilde{E}_d \ll 1$ ,  $r_0(\omega)$  approaches its limiting value from below, while it has an overshoot if  $\delta E/\tilde{E}_d \gg 1$ . In both case the limit value is reached for photoelectron energies of the order of a few times  $\delta E$ .

We then study the effects of the scattering potential by focusing on  $r(\omega)/r_0(\omega)$ . For small energies there is typically an overshoot due to *constructive* interference in the "shake-down" case, contrary to the shake-up case where, like for plasmons,  $r(\omega)/r_0(\omega)$  is reduced by interaction effects. This happens on the energy scale  $\tilde{E}_s$ . If the scattering potential is very strong, this overshoot may extend to several times  $\tilde{E}_s$ . Depending on the parameters there may be an undershoot for higher energies, which can extend up to quite high energies. The undershoot is, however, rather small for the parameters we consider here, and should therefore not be very important unless we want to calculate the spectrum with a high accuracy. For Cu compounds and emission from the  $3s$  core level, we find that  $\tilde{E}_d$  and  $\tilde{E}_s$  are comparable, and the relevant energy for  $r(\omega)/r_0(\omega)$  is then given by  $\tilde{E} \sim \tilde{E}_s \sim \tilde{E}_d$ .

We present our model in Sec. II and calculate various matrix elements in Sec. III. The sudden approximation is described in Sec. IV and exact numerical methods are given in Sec. V. The perturbational and the semi-classical treatments are presented in Sec. VI. In Sec. VII we study the condition for the adiabatic-sudden transition qualitatively, using simple analytic matrix elements and within the framework of the semi-classical theory. The results are discussed in Sec. VIII.

## II. MODEL

We consider a Hamiltonian  $\mathcal{H}_0$  describing a model with a core level  $c$  and two valence levels  $a$  and  $b$ ,

$$\mathcal{H}_0 = \epsilon_a n_a + \epsilon_b n_b + \epsilon_c n_c + U_a n_c n_a + U_b n_c n_b + t(c_a^\dagger c_b + c_b^\dagger c_a). \quad (1)$$

The first two terms give the bare energies of the levels  $a$  and  $b$ , and the last term the hybridization between them. The remaining terms involve the occupation number  $n_c$  of the core level  $c$ . In photoemission the core level is filled in the initial state, and empty in the final, and  $n_c$  only enters as a constant. It is trivial to diagonalize  $\mathcal{H}_0$ , and one obtains two dressed energies  $E_a(n_c)$  and  $E_b(n_c)$  for the levels  $a$  and  $b$ . In a Cu compound, for instance,  $c$

may represent the Cu  $3s$  core level,  $a$  the Cu  $3d$  valence level and  $b$  a ligand state. This is schematically illustrated in Fig. 1. In our calculations we almost always treat the case when  $E_a(1) > E_b(1)$ , and  $E_b(0) > E_a(0)$ . The meaning of the levels  $a$  and  $b$  for different types of systems with localized excitations is indicated in Table I. The full Hamiltonian also has a one-electron part for continuum states,

$$T = \sum_{\mathbf{k}} \epsilon_{\mathbf{k}} n_{\mathbf{k}}, \quad (2)$$

with the energies  $\epsilon_{\mathbf{k}} = k^2/2$ , and wavefunctions  $\psi_{\mathbf{k}}$  obtained from a one-electron potential corresponding to  $n_c = 0$ . The  $n_{\mathbf{k}}$  are occupation numbers  $n_{\mathbf{k}} = c_{\mathbf{k}}^\dagger c_{\mathbf{k}}$ . We use atomic units with  $e = m = \hbar = 1$ , and thus, e.g. energies are in hartrees (27.2 eV). The perturbation causing photoemission is

$$\Delta = \sum_{\mathbf{k}c} (M_{\mathbf{k}} c_{\mathbf{k}}^\dagger c_c + h.c.), \quad (3)$$

where  $M_{\mathbf{k}}$  is an optical transition matrix element. We take the photoelectron interaction as

$$V = \sum_{\mathbf{k}\mathbf{k}'} [n_a V_{\mathbf{k}\mathbf{k}'}^{(a)} + n_b V_{\mathbf{k}\mathbf{k}'}^{(b)} - V_{\mathbf{k}\mathbf{k}'}^{(c)}] c_{\mathbf{k}}^\dagger c_{\mathbf{k}'}. \quad (4)$$

Here  $V_{\mathbf{k}\mathbf{k}'}^{(\nu)}$  is a matrix element of the Coulomb potential  $V^{(\nu)}(\mathbf{r})$  from the charge density  $\rho_\nu(\mathbf{r})$  of the orbital  $\nu$ ,

$$V_{\mathbf{k}\mathbf{k}'}^{(\nu)} = \int \psi_{\mathbf{k}}^*(\mathbf{r}) V^{(\nu)}(\mathbf{r}) \psi_{\mathbf{k}'}(\mathbf{r}) d\mathbf{r}, \quad V^{(\nu)}(\mathbf{r}) = \int \frac{\rho_\nu(\mathbf{r}')}{|\mathbf{r} - \mathbf{r}'|} d\mathbf{r}'.$$

It is the potential  $V$  which determines the transition from the adiabatic to the sudden limit, with  $V = 0$  we are in the sudden limit.

The total Hamiltonian is given by

$$\mathcal{H} = \mathcal{H}_0 + T + V + \Delta. \quad (5)$$

This Hamiltonian has two conserved quantities,

$$n_c + \sum_{\mathbf{k}} n_{\mathbf{k}} = 1 \quad \text{and} \quad n_a + n_b = 1. \quad (6)$$

For simplicity we take the core electron and the  $d$  electron potentials as equal,  $V^c = V^a$ , and use the relation  $n_a + n_b = 1$  to obtain

$$V = n_b \sum_{\mathbf{k}\mathbf{k}'} V_{\mathbf{k}\mathbf{k}'} c_{\mathbf{k}}^\dagger c_{\mathbf{k}'} \quad (7)$$

where

$$V_{\mathbf{k}\mathbf{k}'} \equiv \int \psi_{\mathbf{k}}^*(\mathbf{r}) V_{sc}(\mathbf{r}) \psi_{\mathbf{k}'}(\mathbf{r}) d\mathbf{r},$$

$$V_{sc}(\mathbf{r}) \equiv V^{(b)}(\mathbf{r}) - V^{(a)}(\mathbf{r}) = \int d\mathbf{r}' \frac{1}{|\mathbf{r} - \mathbf{r}'|} [\rho_b(\mathbf{r}') - \rho_a(\mathbf{r}')].$$

The (scattering) potential  $V_{sc}(\mathbf{r})$  describes the change in the potential acting on the emitted electron when the electron in the target hops from level  $a$  to  $b$ .

Dropping a constant we can write  $\mathcal{H}_0$  as

$$\begin{aligned} \mathcal{H}_0 = & \epsilon_c n_c + (\epsilon_a + U n_c) n_a + \epsilon_b n_b \\ & + t(c_a^\dagger c_b + c_b^\dagger c_a). \end{aligned} \quad (8)$$

where the Coulomb integral  $U$  is given by

$$\begin{aligned} U \equiv & U_a - U_b \\ = & \int d\mathbf{r} d\mathbf{r}' \rho_c(\mathbf{r}) \frac{1}{|\mathbf{r} - \mathbf{r}'|} [\rho_a(\mathbf{r}') - \rho_b(\mathbf{r}')]. \end{aligned} \quad (9)$$

Since the core level is very localized in space this leads to

$$U = -V_{sc}(0). \quad (10)$$

For the different types of systems in Table I,  $a$  refers to a localized level and  $b$  refers to a more extended level. For instance, for a copper dihalide compound,  $a$  refers to a Cu 3d orbital and  $b$  to a combination of orbitals on the ligand sites. For simplicity, we approximate the six ligand orbitals by a spherical shell with the radius  $R_0$ ,<sup>20</sup> where  $R_0$  is the average Cu-ligand separation. The potential from the Cu 3d orbital  $V_{3d}(r)$  can be considered as purely Coulombic at  $r = R_0$ . The charge from the spherical shell gives a constant potential inside the radius  $R_0$ , and we have

$$V_{sc}(r) = \begin{cases} (-V_{3d}(r) + \frac{1}{R_0})/\varepsilon & r < R_0; \\ 0 & r > R_0. \end{cases} \quad (11)$$

Here  $\varepsilon$  is a constant chosen to make  $U = -V_{sc}(0)$ , which may be thought of as being due to screening by the surrounding. Since  $V_{3d}(0) \gg 1/R_0$ ,  $\varepsilon$  varies only weakly with  $R_0$  and is approximately given by  $\varepsilon \simeq V_{3d}(0)/U$ .

### III. MATRIX ELEMENTS

To estimate the matrix elements  $M_{\mathbf{k}}$  and  $V_{\mathbf{k}\mathbf{k}'}$  we must approximate the photoelectron wavefunctions  $\psi_{\mathbf{k}}(\mathbf{r})$ . These wavefunctions are calculated from the potential of a neutral atom, which further is shifted to make the potential zero outside a muffin-tin radius  $r_{mt}$ . The states are then described by spherical Bessel functions outside  $r_{mt}$ , which are matched to a solution of the atomic potential inside  $r_{mt}$ . For the energy  $k^2/2$  we obtain the partial wave

$$R_{lk}(r) = \begin{cases} a_{lk} \psi_{lk}(r) & r < r_{mt}; \\ \sqrt{\frac{2}{R}} k [\cos \eta_{lk} j_l(kr) - \sin \eta_{lk} n_l(kr)] & r > r_{mt}, \end{cases} \quad (12)$$

where  $\psi_{lk}(r)$  is the solution of the radial Schrödinger equation for the atomic potential inside the muffin-tin

radius,  $a_{lk}$  is a matching coefficient and  $\eta_{lk}$  a phase shift. The normalization is given by

$$\int_0^R dr r^2 R_{lk}^2(r) = 1, \quad (13)$$

where  $R$  is the radius of a large sphere to which the continuum states are normalized. The factor  $(2/R)^{1/2}k$  is due to the normalization and the asymptotic behavior of  $j_l(x)$  for large  $x$ .

Slater's rules<sup>21</sup> are used to generate the orbitals and charge densities, from which the potential  $V_{3d}(r)$  is calculated. This gives the scattering potential  $V_{sc}(r)$ , which is shown in Fig. 2a. We consider photoemission from a Cu 3s hole. Due to the dipole selection rules, the core electron is then emitted into a continuum state of  $p$ -symmetry. The matrix elements  $V_{kk'}$  of the scattering potential  $V_{sc}(r)$  are shown in Fig. 2b,

$$V_{kk'} = \int dr r^2 R_k(r) V_{sc}(r) R_{k'}(r), \quad (14)$$

where the muffin-tin radius  $r_{mt}$  is taken as the ionic radius of Cu,  $r_{mt} = 2.6$  a.u., and we have dropped the  $l$  index, since we always consider  $l = 1$ . The dipole matrix element  $M_k$  is given by

$$M_k \sim a_k (\epsilon_k - \epsilon_c) \int dr r^2 \psi_{3s}(r) r \psi_k(r). \quad (15)$$

We assume that the core level is deep, and  $|\epsilon_c|$  much larger than the energy difference between the ligand and copper levels. We can then take the factor  $\epsilon_k - \epsilon_c$  as a constant, which drops out since we always consider relative intensities. The result for  $M_k$  is shown as the solid line in Fig. 3a. These dipole and scattering potential matrix elements are used in the following numerical calculations. Extensive calculations of dipole matrix elements for many systems were performed by Yeh and Lindau.<sup>22</sup>

To interpret the results, it is useful to also perform analytical calculations. For this purpose we need models of the matrix elements. Below we consider the limits of low and high kinetic energies of the emitted electron. In the limit of low kinetic energies, we replace the spherical Bessel function by its expansion for small arguments

$$j_l(x) = \frac{1}{(2l+1)!!} x^l, \quad n_l(x) = -(2l-1)!! \frac{1}{x^{l+1}} \quad (16)$$

and the solution  $\psi_{lk}(r)$  by its zero energy limit  $\psi_{l0}(r)$ . This leads to

$$\begin{aligned} \tan \eta_{lk} &= \frac{l - \xi}{l + 1 + \xi} \frac{(kr_{mt})^{2l+1}}{(2l-1)!!(2l+1)!!} \sim \eta_{lk}, \\ a_{lk} &= \sqrt{\frac{2}{R}} k \left[ \frac{2l+1}{l+1+\xi} \frac{(kr_{mt})^l}{(2l+1)!!} \right] \frac{1}{\psi_{l0}(r_{mt})}. \end{aligned} \quad (17)$$

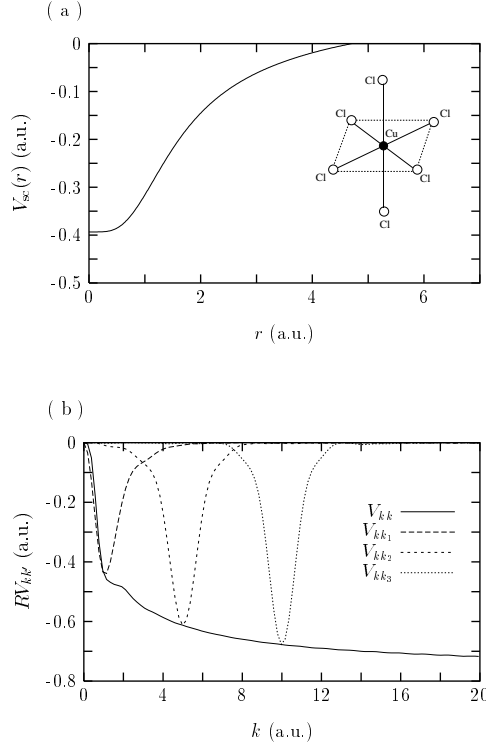


FIG. 2. (a) The photoelectron scattering potential  $V_{sc}(r)$  given by Eq. (11) with respect to  $r$  for  $\text{CuCl}_2$  ( $R_0 = 4.71$  a.u. and  $\epsilon = 1.96$ ). In the inset, we give the atomic configuration of Cu-Cl octahedral (nearly octahedral) cluster in  $\text{CuCl}_2$ . (b) The diagonal and off-diagonal matrix elements of the scattering potential multiplied by  $R$ . In the figure,  $k_1 = 1$  a.u.,  $k_2 = 5$  a.u., and  $k_3 = 10$  a.u. are taken.

Due to the matching, the coefficient  $a_{lk}$  contains the ratio  $\xi = r_{mt}\psi'_{l0}(r_{mt})/\psi_{l0}(r_{mt})$ . The value of the coefficient therefore depends in an interesting way on the wave function  $\psi_{l0}$  and its derivative, and if  $l+1+\xi$  is close to zero  $a_{lk}$  blows up. Then the matrix elements of the scattering potential also blow up and we may expect strong deviations from the sudden approximation. In such a case the dipole matrix element  $M_{lk}$  also becomes large, i.e., there is a resonance ( $\eta_{lk} = \frac{\pi}{2}$ ) in the photoemission cross section.

From Eqs.(12) and (15) it follows that in the limit of a small  $k$  the dipole matrix element is proportional to  $a_k \sim k^{l+1}$ . The main peak and the satellites in the photoemission spectrum correspond to different kinetic energies and therefore have dipole matrix elements with different  $k$ -values. This is important at low energies, while for large energies the variation in  $M_{lk}$  is generally small over a range of the energy difference between the main peak and the satellite, and for the ratio of the peaks, the dipole matrix elements should then not play a role. For simplicity, we assume that the dipole matrix elements become independent of  $k$  for  $\tilde{R}_d k \gg 1$ , where  $\tilde{R}_d$  is some typical length scale of the system. For our case ( $l = 1$ )

we use the model (note that any constant factor in  $M_k$  drops out in our final expressions)

$$M_k = \frac{(\tilde{R}_d k)^2}{1 + (\tilde{R}_d k)^2} \equiv \frac{\epsilon_k/\tilde{E}_d}{1 + \epsilon_k/\tilde{E}_d}, \quad (18)$$

where  $\tilde{E}_d = 1/(2\tilde{R}_d^2)$ . Fig. 3a compares this model with the full calculation for a  $3s$  orbital. We obtain  $\tilde{R}_d = 1.3$  a.u.. For a  $1s$  or  $2s$  orbital the length scale is smaller and  $\tilde{R}_d \sim 1/2$  a.u.. While we consider  $l = 1$  the behaviour for other  $l$  is primarily modified for small energies.

We next consider the matrix elements  $V_{kk'}$ . For small values of  $k$  and  $k'$  and for  $l = 1$

$$V_{kk'} = \frac{2}{R} \left[ \frac{r_{mt}}{\psi_{l0}(r_{mt})} \right]^2 \frac{(kk')^2}{(\xi + 2)^2} \int_0^{r_{mt}} \psi_{l0}^2(r) V_{sc}(r) r^2 dr + \frac{2}{9R} (kk')^2 \int_{r_{mt}}^{R_0} \left[ r + \left( \frac{1-\xi}{2+\xi} \right) \frac{r_{mt}^3}{r^2} \right]^2 V_{sc}(r) r^2 dr. \quad (19)$$

For small values of  $k$  and  $k'$  it then follows that  $V_{kk'} \sim (kk')^2$ . For large values of  $k$  and  $k'$  the matrix elements become very small due to destructive interference between the two wave-functions unless  $k \approx k'$ . If  $k = k'$  the matrix elements  $V_{kk}$  approach a constant. These features are contained in the model

$$V_{kk'} = \frac{\tilde{V}\tilde{R}_s}{R} \frac{(\tilde{R}_s^2 kk')^2}{[1 + (\tilde{R}_s k)^2][1 + (\tilde{R}_s k')^2][1 + \tilde{R}_{sd}^2(k - k')^2]}, \quad (20)$$

where  $\tilde{R}_s$  and  $\tilde{R}_{sd}$  are appropriate length scales and  $\tilde{V}$  has the energy dimension. We recall that  $\tilde{V}$  contains information about the coefficient  $a_{lk}$  defined in Eq.(17) and therefore about the atomic potential and that  $\tilde{V}$  may become particularly large close to a resonance. The dipole matrix element  $M_k$  and potential matrix  $V_{kk'}$  in our simplified model Eqs. (18) and (20) are given in Fig. 3 as compared with the exact results.

For large values of  $k$  and  $k'$ , the expression Eq. (20) simplifies to

$$V_{kk'} = \frac{\tilde{V}\tilde{R}_s}{R} \frac{1}{1 + \tilde{R}_{sd}^2(k - k')^2}. \quad (21)$$

An expression of this type can also be derived by assuming that the wave functions  $R_{lk}(r)$  can be approximated by spherical Bessel functions in all of space, and by assuming some shape of  $V_{sc}(r)$ , e.g., a linear dependence on  $r$

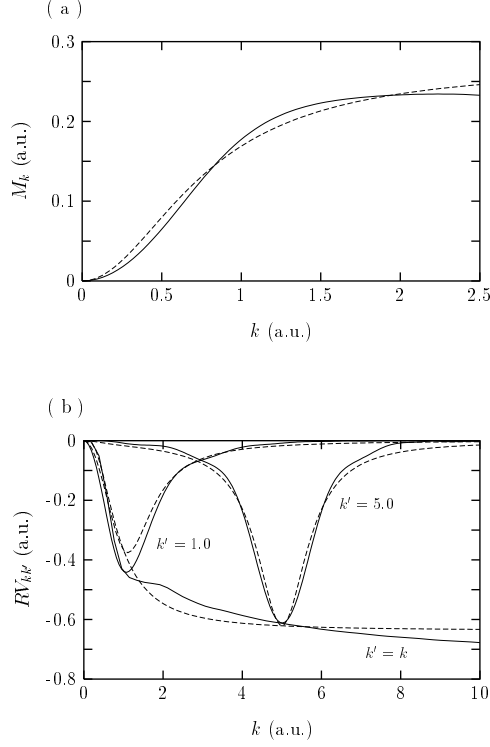


FIG. 3. (a) The dipole matrix element  $M_k$  as a function of  $k$ . The exact result (solid line) is obtained from Eq. (15) and the simplified model by Eq. (18) is also shown (dashed line). The appropriate parameter is  $\tilde{R}_d = 1.30$  a.u. (b) The matrix elements  $V_{kk'}$  of the scattering potential are given for  $k = k'$ ,  $k' = 1$  a.u., and  $k' = 5$  a.u.. The solid line is from the exact calculation for the model of  $\text{CuCl}_2$  and the dashed line is based on the simplified model (Eq.(20)). The parameters are  $\tilde{V} = -0.36$  a.u.,  $\tilde{R}_s = 1.77$  a.u. and  $\tilde{R}_{sd} = 1.31$  a.u..

$$V_{sc}(r) = V_{sc}(0)\left(1 - \frac{r}{R_0}\right). \quad (22)$$

For large values of  $k$  and  $k'$  we then obtain

$$V_{kk'} = \frac{V_{sc}(0)R_0}{R} \frac{1 - \cos[(k - k')R_0]}{[(k - k')R_0]^2}. \quad (23)$$

For this model we relate  $\tilde{R}_s = \tilde{R}_{sd} = R_0/3$  to the range  $R_0$  of the potential and  $\tilde{V} = 3V_{sc}(0)/2$ . Using this identification in Eq. (21), leads to the correct average value of  $V_{kk}$  and to the correct width in  $k - k'$  of  $V_{kk'}$ . The simple form (21), however, neglects the effects of the oscillations of the cos-function in Eq. (23) for large values of  $(k - k')R_0$ , and it therefore gives a worse representation of the linear potential (22) than the form (20) gives for the more realistic scattering potential (11). Later we will find that it is a reasonable approximation to put  $\tilde{R}_d$ ,  $\tilde{R}_{sd}$  and  $\tilde{R}_s$  equal to the same value  $\tilde{R}$ , and introduce the corresponding energy  $\tilde{E} = 1/(2\tilde{R}^2)$ .

#### IV. SUDDEN APPROXIMATION

We first discuss the photoemission in the sudden limit, i.e., we neglect the scattering potential between the emitted electron and the target ( $V \equiv 0$ ). The initial state  $|\Psi_0\rangle$  is the ground state of  $\mathcal{H}_0$  with  $n_c = 1$  and given by

$$|\Psi_0\rangle = -\sin\theta|\psi_c\rangle|\psi_a\rangle + \cos\theta|\psi_c\rangle|\psi_b\rangle, \quad (24)$$

where

$$\tan 2\theta = 2t/(\epsilon_a + U - \epsilon_b) \quad (25)$$

and the corresponding ground state energy is

$$E_0 = \epsilon_c + \frac{1}{2}(\epsilon_a + U + \epsilon_b) - \frac{1}{2}\sqrt{(\epsilon_a + U - \epsilon_b)^2 + 4t^2}. \quad (26)$$

The final states of the target are given by the two eigenstates of  $\mathcal{H}_0$  with  $n_c = 0$

$$\begin{aligned} |\psi_1\rangle &= \cos\varphi|\psi_a\rangle - \sin\varphi|\psi_b\rangle, \\ |\psi_2\rangle &= \sin\varphi|\psi_a\rangle + \cos\varphi|\psi_b\rangle, \end{aligned} \quad (27)$$

with

$$\tan 2\varphi = 2t/(\epsilon_b - \epsilon_a) \quad (28)$$

and the corresponding energy eigenvalues  $E_1$  and  $E_2$  are

$$E_{1,2} = \frac{1}{2}(\epsilon_a + \epsilon_b) \mp \delta E/2, \quad (29)$$

with

$$\delta E = \sqrt{(\epsilon_a - \epsilon_b)^2 + 4t^2} \quad (30)$$

being the optical excitation energy of the system.

The photocurrent  $J_k^s(\omega)$  ( $s = 1, 2$ ) is given by,<sup>1</sup>

$$J_k^s(\omega) = |\langle \Psi_f^{sk} | \Delta | \Psi_0 \rangle|^2 \delta(\omega - \epsilon_k + E_0 - E_s), \quad (31)$$

where  $|\Psi_f^{sk}\rangle$  is a final state. According to the sudden approximation, it can be written as the final target state multiplied by the photoelectron state,  $|\Psi_f^{sk}\rangle = |\psi_s\rangle|\psi_k\rangle$ . This gives

$$\langle \Psi_f^{sk} | \Delta | \Psi_0 \rangle = M_k w_s \equiv m_{sk}, \quad w_s = \begin{cases} -\sin(\varphi + \theta), & s = 1 \\ \cos(\varphi + \theta), & s = 2 \end{cases} \quad (32)$$

$J_k^1(\omega)$  gives the main line (corresponding to the quasi particle line in metal) and  $J_k^2(\omega)$  the satellite line. The schematic picture of the initial and final state for this system is given in Fig. 1. Summing the kinetic energy distribution of the photoelectron, we obtain the absorption spectra  $J_s(\omega)$ ,

$$J_s(\omega) = \sum_k J_k^s(\omega) \propto \frac{1}{k_s} |M_{k_s} w_s|^2$$

$$k_s = \sqrt{2(\omega + E_0 - E_s)}, \quad (33)$$

where the threshold energies for  $J_1(\omega)$  and  $J_2(\omega)$  are given by  $E_1 - E_0$  and  $E_2 - E_0 (\equiv \omega_{th})$ , respectively. We can thus also write  $k_1 = \sqrt{2(\omega + \delta E - \omega_{th})}$  and  $k_2 = \sqrt{2(\omega - \omega_{th})}$ . The factor  $1/k$  comes from the  $k$ -summation over a  $\delta$ -function in energy. For convenience we introduce the quantity  $\tilde{\omega} = \omega - \omega_{th}$ , and thus  $\epsilon_{k_2} = \tilde{\omega}$ .

In the sudden approximation the kinetic energy of the emitted electron is large, and we can take  $k_1 = k_2$ . The ratio  $r_{00}$  of the satellite to the main peak intensity then is

$$r_{00} = \lim_{\omega \rightarrow \infty} \frac{J_2(\omega)}{J_1(\omega)} = \cot^2(\varphi + \theta). \quad (34)$$

Taking into account the energy dependence of the dipole matrix element according to model Eq. (18) as well as the factor  $1/k$ , we obtain

$$r_0(\omega) = r_{00} \left[ \frac{\tilde{\omega}}{\tilde{\omega} + \delta E} \right]^{\frac{3}{2}} \times \left[ \frac{1 + (\tilde{\omega} + \delta E)/\tilde{E}_d}{1 + \tilde{\omega}/\tilde{E}_d} \right]^2 \Theta(\tilde{\omega}). \quad (35)$$

We now require that the ratio  $r_0(\omega)$  should reach a fraction  $\gamma$  ( $\gamma \approx 1$ ) of its limiting value  $r_0(\infty)$  for  $\omega = \omega_\gamma$ . This gives

$$\frac{\omega_\gamma - \omega_{th}}{\delta E} \approx \begin{cases} \frac{3}{2} \frac{1}{1-\gamma}, & \text{if } \delta E \ll \tilde{E}_d; \\ \gamma^{2/3} (\tilde{E}_d / \delta E)^{4/3}, & \text{if } \delta E \gg \tilde{E}_d. \end{cases} \quad (36)$$

This criterion refers to the energy where  $r_0(\omega)$  reaches a fraction  $\gamma$  in its rising part, and it does not consider that there is a large overshoot for  $\delta E / \tilde{E}_d \gg 1$ . In this case we can instead require that  $r_0(\omega)$  is smaller than  $\gamma \approx 1$  in its descending part. This gives the condition

$$\frac{\omega_\gamma - \omega_{th}}{\delta E} \approx \frac{1}{\gamma^2 - 1} \quad \delta E / \tilde{E}_d \gg 1, \gamma > 1. \quad (37)$$

In Fig. 4 we show results for  $r_0(\omega)$  over a large range of values for  $\delta E / \tilde{E}$ . The figure illustrates that the dipole matrix element effect alone makes the sudden approximation invalid for small kinetic energies. It is interesting that for somewhat larger photon energies  $r_0$  overshoots. The reason is that the matrix elements  $M_k$  saturate for  $\epsilon_k \gg \tilde{E}_d$ , while the factor  $1/k$  in Eq.(33) favors the satellite. For  $\delta E / \tilde{E}_d = 1$ , the result is rather close to the sudden limit for  $\tilde{\omega} / \delta E \sim 1$ . Finally, for  $\delta E / \tilde{E}_d \gg 1$ , there is a substantial overshoot.

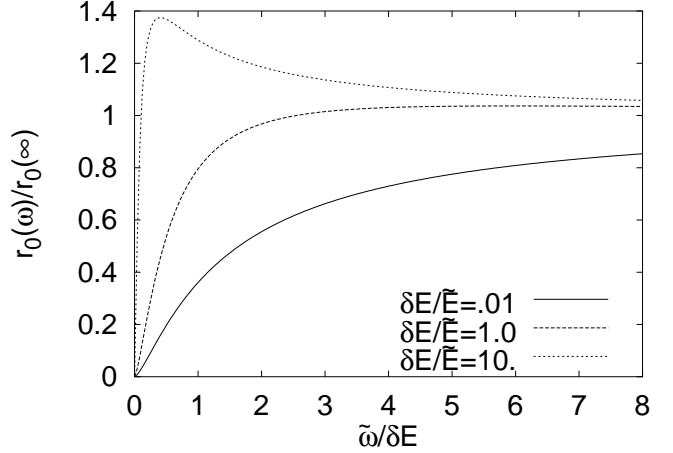


FIG. 4. The ratio  $r_0(\omega)$  of the satellite to the main peak in Eq.(35) divided by the result for an infinite photon energy ( $r_0(\infty) = r_{00}$ ). Three values of the excitation energy  $\delta E$  are considered.

As discussed in the introduction, we would like to study how the adiabatic to sudden transition depends on certain factors, like the range  $R_0$  of the potential and the energy  $\delta E$  of the excitation causing the satellite. We therefore keep ratio of  $t, U$  and  $\epsilon_a - \epsilon_b$  fixed, but vary their magnitude. In this way we can vary  $\delta E$  without varying the magnitude of the satellite in the sudden limit. Eq. (10) requires that we vary  $V_{sc}(0)$  as we vary  $\delta E$  (via  $U$ ), e.g., by varying the dielectric constant  $\epsilon$ . In some of the calculations below, however, we do not impose Eq. (10), to be able to see the effect of varying  $\delta E$  alone. We furthermore vary the range  $R_0$  of the potential. From the definition Eq. (11) it follows that this would also vary the strength of the potential. For this reason we simultaneously vary the dielectric constant  $\epsilon$  so that  $V_{sc}(0)$  stays unchanged when  $R_0$  is changed. Alternatively, we can use the analytical matrix elements (18, 20). We can then easily vary the length scale by changing  $\tilde{R}$  or the strength by changing  $\tilde{V}$ .

To know roughly what are interesting values for our parameters we use experimental results for some copper dihalides.<sup>15</sup> We estimate the relative strength of the satellite to the main peak, and the energy difference between the peaks. This gives two equations while in our model these quantities,  $r_{00}$  and  $\delta E$ , depend on three parameters,  $t, U$ , and  $\epsilon_a - \epsilon_b$ . To only have two parameters we consider *the symmetric case*  $\epsilon_a = \epsilon - U/2$  and  $\epsilon_b = \epsilon$  as shown in Fig.1. In the symmetric case we are restricted to the shake-down situation since before the transition the  $a$ -level is above the  $b$ -level,  $\epsilon_a + U - \epsilon_b = U/2$ , while after the transition the  $a$ -level is below the  $b$ -level,  $\epsilon_b - \epsilon_a = U/2$ . In the symmetric case we have  $0 < \theta = \varphi < \pi/4$ , and  $r_{00} = \cot^2 2\varphi = U^2 / (16t^2)$ . Once we know where in the ball-park we have  $t$  and  $U$ , we can leave the symmetric case, and also consider, e.g., shake-up cases when there is no level crossing,  $\epsilon_a > \epsilon_b$ . In the

lowest final state the electron essentially stays on level  $b$ , while the transfer of the electron to the level  $a$  corresponds to a shake up satellite. In this case we have  $-\pi/4 < \varphi < 0 < \theta < \pi/4$  and  $\varphi + \theta < 0$ .

Our calculations usually take the  $\text{CuCl}_2$  parameters as reference values. For  $\text{CuCl}_2$  we have  $\theta = \varphi = 0.3$ , which gives  $r_{00} = 2.1$ . Further  $\tilde{V} = -0.36$  a.u.,  $\tilde{E} = 0.195$  a.u. (with  $\tilde{R} = 1.6$  a.u.), and  $\delta E = 0.237$  a.u., i.e.,  $\tilde{V}/\tilde{E} = -1.85$  and  $\delta E/\tilde{V} = -0.66$  (see also Table II).

## V. EXACT TREATMENT

### A. Time-dependent formulation

To obtain exact results for model Eq.(5), we use a time-dependent formulation<sup>23</sup> and solve the Schrödinger equation for the Hamiltonian

$$\mathcal{H}(\tau) = \mathcal{H}_0 + T + V + \Delta f(\tau). \quad (38)$$

The interaction is switched on at  $\tau = 0$ , using

$$f(\tau) = e^{-i\omega\tau}(e^{-\eta\tau} - 1) \quad \eta > 0. \quad (39)$$

Here  $\eta$  is a small quantity to assure that the external field is switched on smoothly. The initial ( $\tau = 0$ ) state  $|\Psi_0\rangle$  is given by the ground state of  $\mathcal{H}_0$  with  $n_c = 1$  in Eq.(1). After a time  $\tau$ , the state  $|\Psi(\tau)\rangle$  of the system is

$$|\Psi(\tau)\rangle = a(\tau)|\psi_a\rangle|\psi_c\rangle + b(\tau)|\psi_b\rangle|\psi_c\rangle + \sum_k c_{ak}(\tau)|\psi_a\rangle|\psi_k\rangle + \sum_k c_{bk}(\tau)|\psi_b\rangle|\psi_k\rangle. \quad (40)$$

The coefficients of  $|\Psi(\tau)\rangle$  can be determined by

$$i\frac{\partial}{\partial\tau}|\Psi(\tau)\rangle = \mathcal{H}(\tau)|\Psi(\tau)\rangle, \quad (41)$$

which gives four differential equations for the four coefficients  $a(\tau)$ ,  $b(\tau)$ ,  $c_{ak}(\tau)$ , and  $c_{bk}(\tau)$ ,

$$i\frac{\partial}{\partial\tau}a(\tau) = (\epsilon_a + U + \epsilon_c)a(\tau) + tb(\tau) + \sum_k V_k^{d*}(\tau)c_{ak}(\tau), \quad (42)$$

$$i\frac{\partial}{\partial\tau}b(\tau) = (\epsilon_b + \epsilon_c)b(\tau) + ta(\tau) + \sum_k V_k^{d*}(\tau)c_{bk}(\tau), \quad (43)$$

$$i\frac{\partial}{\partial\tau}c_{ak}(\tau) = (\epsilon_a + \epsilon_k)c_{ak}(\tau) + tc_{bk}(\tau) + V_k^d(\tau)a(\tau), \quad (44)$$

$$i\frac{\partial}{\partial\tau}c_{bk}(\tau) = (\epsilon_b + \epsilon_k)c_{bk}(\tau) + tc_{ak}(\tau) + V_k^d(\tau)b(\tau) + \sum_{k'} V_{kk'}c_{bk'}(\tau), \quad (45)$$

where  $V_k^d(\tau) = V_0 M_k f(\tau)$  with  $V_0$  representing the strength of the external field. We solve the equations in the limit when  $V_0 \rightarrow 0$ , and thus the ratio between  $c_{ak}$  and  $c_{bk}$  is independent of  $V_0$ . The initial conditions are  $a(0) = -\sin\theta$ ,  $b(0) = \cos\theta$ , and  $c_{ak}(0) = c_{bk}(0) = 0$ . Thus the problem is reduced to solving the coupled differential equations, which is done using the Runge-Kutta fourth-order method.

The photoelectron currents  $J_1(\omega)$  and  $J_2(\omega)$  corresponding to main and satellite lines, respectively, are given by

$$J_1(\omega) = \sum_k |\langle \Psi_f^{1k} | \Psi(\tau) \rangle|^2 = \sum_k |\cos\varphi c_{ak}(\tau) - \sin\varphi c_{bk}(\tau)|^2, \quad (46)$$

$$J_2(\omega) = \sum_k |\langle \Psi_f^{2k} | \Psi(\tau) \rangle|^2 = \sum_k |\sin\varphi c_{ak}(\tau) + \cos\varphi c_{bk}(\tau)|^2, \quad (47)$$

where  $\tau$  is a sufficiently large time. We let the system evolve for a time of the order  $1/\eta$  to obtain converged results for a given finite  $V_0$ . In principle, we should perform the calculation for a few small values of  $\eta$  and then extrapolate to  $\eta = 0$  followed by an extrapolation  $V_0 \rightarrow 0$ . Here, for simplicity we have performed the calculation for one single small value of  $V_0$ . The calculation was performed for  $\eta = 0.1$  eV, 0.08 eV, 0.02 eV, and the results were extrapolated to  $\eta = 0$  assuming the  $\eta$  dependence  $a(\omega)\eta + b(\omega)\eta^2 + c(\omega)$ . The error in this approach occurs primarily for small  $\tilde{\omega}$  ( $\lesssim 5$  eV), and it is then less than 5% in  $r(\omega)/r_0(\omega)$ .

The approach above gives the relative intensity of the main and satellite peaks

$$r(\omega) = \frac{J_2(\omega)}{J_1(\omega)}. \quad (48)$$

It can be shown that the formulas (46, 47) above give identical results to the more conventional formulation (51) below, by performing derivations of the type made in, e.g., Ref. 24.

As an example of the results obtained in this formalism, we show in Fig. 5 results for the copper dihalides  $\text{CuBr}_2$ ,  $\text{CuCl}_2$  and  $\text{CuF}_2$ . The corresponding parameters are shown in Table II and were estimated from experiment.<sup>15</sup> The figure illustrates that there is a small ‘‘overshoot’’ for small  $\tilde{\omega}$  but that the sudden limit is reached fairly quickly as  $\tilde{\omega}$  is further increased. We remind that in our  $\text{CuCl}_2$  reference case  $\tilde{E}=0.195$  a.u.=5.3 eV.



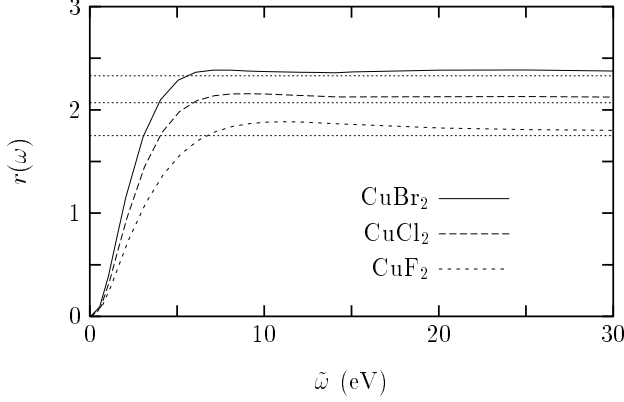


FIG. 5. The ratio  $r(\omega)$  between the satellite and the main peak for the divalent copper compounds  $\text{CuBr}_2$ ,  $\text{CuCl}_2$ , and  $\text{CuF}_2$ . The parameters are given in Table II. The dotted lines are the limit values ( $r(\infty)$ ) for the respective cases.

### B. Resolvent formulation

Alternatively, we can work in the energy space, and obtain the spectrum by direct inversion of a resolvent operator. We consider the Hamiltonian  $\mathcal{H}$ ,

$$\mathcal{H} = \mathcal{H}_0 + T + V, \quad (49)$$

where by  $\mathcal{H}_0$  we understand  $\mathcal{H}_0(n_c = 0)$ . The exact final photoemission state  $|\Psi_f^{sk}\rangle$  is<sup>1</sup>

$$|\Psi_f^{sk}\rangle = \left[ 1 + \frac{1}{E - \mathcal{H}_0 - T - V - i\eta} V \right] |\psi_s\rangle |\psi_k\rangle, \quad (50)$$

where  $|\psi_s\rangle$  ( $s = 1, 2$ ) (Eq. (27)) are the exact (target) eigenstates of  $\mathcal{H}_0(n_c = 0)$  and  $E = \epsilon_k + E_s$  is the energy of the final state. Using Eq. (50) we calculate the matrix element  $M(s, k) \equiv \langle \Psi_f^{sk} | \Delta | \Psi_0 \rangle$

$$\begin{aligned} M(s, k) & \quad (51) \\ &= \langle \psi_k | \langle \psi_s | \left[ 1 + V \frac{1}{\epsilon_k + E_s - \mathcal{H}_0 - T - V + i\eta} \right] \Delta | \Psi_0 \rangle. \end{aligned}$$

Introducing a basis set

$$|i\rangle = |\psi_s\rangle |\psi_k\rangle, \quad (52)$$

the matrix elements of  $V$  can then be written as

$$V_{ij} \equiv V_{k_s, k'_s s'} = V_{k k'} v_s v_{s'}. \quad (53)$$

Here

$$v_s = \begin{cases} -\sin\varphi, & \text{if } s = 1; \\ \cos\varphi, & \text{if } s = 2, \end{cases} \quad (54)$$

where we have used Eqs. (7, 27). The Hamiltonian matrix in this basis set is diagonalized, which gives the eigenvalues  $\epsilon_\nu$  and the eigenvectors

$$|\nu\rangle = \sum_i c_i^\nu |i\rangle. \quad (55)$$

We then have

$$\begin{aligned} M(s, k) & \equiv M(i) = & (56) \\ \langle i | \Delta | \Psi_0 \rangle &+ \sum_\nu \sum_{j,l} \frac{V_{i,j} c_j^\nu c_l^\nu \langle l | \Delta | \Psi_0 \rangle}{\epsilon_k + E_s - \epsilon_\nu + i\eta}. \end{aligned}$$

The quantities  $\langle i | \Delta | \Psi_0 \rangle$  were given in Eq. (32),  $\langle i | \Delta | \Psi_0 \rangle = m_i = m_{sk} = M_k w_s$ . By organizing the sums in Eq. (56) appropriately, the calculation of this expression is very fast and the main time is spent in diagonalizing the Hamiltonian matrix. We have found this method to be more efficient than the time-dependent method above.

In the expression (56), we can identify the first term as the intrinsic contribution, since this is the amplitude which is obtained if there is no interaction between the photoelectron and the target. The extrinsic effects are then determined by the square of the absolute value of the second term. The interference between the intrinsic and extrinsic contributions is given by the cross product of these terms.

### C. Separable potential

It is interesting to consider a separable potential

$$V_{kk'} = \tilde{V} b_k b_{k'}, \quad (57)$$

since it is then possible to obtain an analytical expression for  $r(\omega)$ . The operator in the denominator of Eq. (50) is written as

$$(z - \mathcal{H}_0 - T - V)_{ij} = d_i(z) \delta_{ij} - \tilde{V} c_i c_j, \quad (58)$$

where again  $|i\rangle = |s\rangle |k\rangle$  is a combined index for the target state  $s$  and the continuum state  $k$  and  $z$  is a (complex) number. Then

$$d_{sk}(z) \equiv d_i(z) = z - E_s - \epsilon_k \quad (59)$$

and

$$c_i \equiv c_{sk} = b_k v_s. \quad (60)$$

Using the fact that  $V$  is separable, it is then straightforward to invert the expression in Eq. (58) and obtain

$$\begin{aligned} & [(z - \mathcal{H}_0 - T - V)^{-1}]_{ij} & (61) \\ &= \frac{\delta_{ij}}{d_i(z)} + \tilde{V} \frac{c_i c_j}{d_i(z) d_j(z) (1 - \tilde{V} \sum_l c_l^2 / d_l(z))}. \end{aligned}$$

This leads to

$$\frac{r(\omega)}{r_0(\omega)} = \left| \frac{1 + \cos\varphi D_{k_2}(E_0 + \omega)/\cos(\varphi + \theta)}{1 + \sin\varphi D_{k_1}(E_0 + \omega)/\sin(\varphi + \theta)} \right|^2, \quad (62)$$

where  $k_s$  is defined in Eq. (33),

$$D_k(\epsilon) = -\frac{\tilde{V}}{\tilde{E}_s} \frac{b_k E(\epsilon)}{M_k [1 + (\tilde{V}/\tilde{E}_s)C(\epsilon)]}, \quad (63)$$

with  $\tilde{E}_s = 1/(2\tilde{R}_s^2)$  and

$$C(\epsilon) = -\tilde{E}_s \sum_l \frac{c_l^2}{d_l(\epsilon + i\eta)} \quad (64)$$

and

$$E(\epsilon) = -\tilde{E}_s \sum_l \frac{c_l m_l}{d_l(\epsilon + i\eta)}. \quad (65)$$

To obtain a model for  $V_{kk'}$  we can, for instance, put

$$b_k = \sqrt{\frac{\tilde{R}_s}{R}} \frac{(\tilde{R}_s k)^2}{1 + (\tilde{R}_s k)^3}. \quad (66)$$

Compared with the expression in Eq. (20), there is no term  $k-k'$  in the corresponding expression for  $V_{kk'}$ . The neglect of this term means that  $V_{kk'}$  goes to zero more slowly as one of the arguments  $k$  or  $k'$  goes to infinity. To compensate for this we use the power three for  $\tilde{R}_s k$  in the denominator of (66), while in Eq. (20) the corresponding power is two. This is a reasonable approximation for small  $k$ , but it breaks down for large  $k$ .

#### D. On the variables in the intensity ratio

For the satellite to main line intensity ratio we have,

$$r(\omega) = \frac{k_1}{k_2} \left| \frac{M(2, k_2)}{M(1, k_1)} \right|^2.$$

This ratio does not depend on any constant factor in  $M_k$ , since  $M(s, k)$  is proportional to  $M_k$ . If we take the parameters  $\tilde{R}_d$ ,  $\tilde{R}_s$ , and  $\tilde{R}_{sd}$  equal to a common typical radius  $\tilde{R}$  (as will be motivated later), and use the analytic expressions in Eqs. (18) and (20) then  $r(\omega)$  or  $r(\omega)/r_0(\omega)$ , apart from  $\varphi$  and  $\theta$ , becomes a function of  $\delta E/\tilde{E}$ ,  $\tilde{V}/\tilde{E}$ , and  $\tilde{\omega}/\tilde{E}$ , with  $\tilde{E} = (2\tilde{R}^2)^{-1}$ . We can see this since  $M_k$  is a function of  $k\tilde{R}$ , and  $V_{kk'}$  a function of  $k\tilde{R}$  and  $k'\tilde{R}$  apart from their prefactors. The prefactor of  $V_{kk'}$  is  $\tilde{V}\tilde{R}/R$ , while that for  $M_k$  has no influence. For each  $V$  in a perturbation expansion of Eq. (51) we have an energy denominator and a  $k$ -summation. The  $k$ -summation gives an integral and a factor  $Rdk$ . Using variables  $\tilde{R}k$ , the  $\tilde{R}/R$  in the prefactor vanishes. Factoring out  $\tilde{E}$  in the energy denominator, we have a factor

$\tilde{V}/\tilde{E}$  for each  $V_{kk'}$ , and instead of  $\delta E$  and  $\tilde{\omega}$  we have  $\delta E/\tilde{E}$  and  $\tilde{\omega}/\tilde{E}$ .

With  $\theta$  and  $\varphi$  given,  $\delta E$  is proportional to  $U$ .  $U$  in turn is equal to  $-V_{sc}(0)$ , and thus somehow related to the strength of the scattering potential  $\tilde{V}$ . If we fix the value of the sudden limit  $r_{00} = \cot^2(\varphi + \theta)$  by choosing one of the angles, we still have an independent parameter left. This parameter can be used to decouple the relation between  $\delta E$  and  $\tilde{V}$  (whatever it is). Summarizing, we have found that the parameters of our model system appear as the angles  $\theta$  and  $\varphi$ , and the excitation energy  $\delta E$  (or  $U$ ), while the coupling between the photoelectron and the model system only appears in one parameter,  $\tilde{V}/\tilde{E} = 2\tilde{V}\tilde{R}^2$ , provided we use  $\tilde{\omega}/\tilde{E}$  as variable. We have further motivated that we can vary the parameters  $\delta E$  and  $\tilde{V}$  independently.

## VI. APPROXIMATE TREATMENTS

### A. Perturbation approach to lowest order in $V_{kk'}$

The same problem can be also studied using the standard perturbation approach. We consider the expression for the matrix elements  $M(s, k)$  in Eq. (51). To lowest order in  $V$ , we can neglect  $V$  in the denominator of Eq. (51). Inserting the completeness relation  $\sum_i |i\rangle\langle i| = 1$  in terms of eigenstates  $|i\rangle \equiv |k\rangle|s\rangle$  we obtain

$$M(s, k) = \langle s| \langle k| \Delta | \Psi_0 \rangle + \sum_{k's'} V_{ks, k's'} [(E - \mathcal{H}_0 - T + i\eta)^{-1}]_{k's', k's'} \langle s' | \langle k' | \Delta | \Psi_0 \rangle. \quad (67)$$

Using Eqs. (53, 54) we obtain

$$M(1, k) = -\sin(\varphi + \theta)M_k - \sin^2 \varphi \sin(\varphi + \theta) \sum_{k'} \left[ \frac{V_{kk'} M_{k'}}{E - E_1 - \epsilon_{k'} + i\eta} \right] - \frac{\sin 2\varphi \cos(\varphi + \theta)}{2} \sum_{k'} \left[ \frac{V_{kk'} M_{k'}}{E - E_2 - \epsilon_{k'} + i\eta} \right], \quad (68)$$

$$M(2, k) = \cos(\varphi + \theta)M_k + \cos^2 \varphi \cos(\varphi + \theta) \sum_{k'} \left[ \frac{V_{kk'} M_{k'}}{E - E_2 - \epsilon_{k'} + i\eta} \right] + \frac{\sin 2\varphi \sin(\varphi + \theta)}{2} \sum_{k'} \left[ \frac{V_{kk'} M_{k'}}{E - E_1 - \epsilon_{k'} + i\eta} \right], \quad (69)$$

where  $V_{kk'} = \langle k|V_{sc}|k'\rangle$  and  $M_k = \langle k|\Delta|\psi_c\rangle$ . We can then immediately calculate the photoemission spectra using Eq. (31).

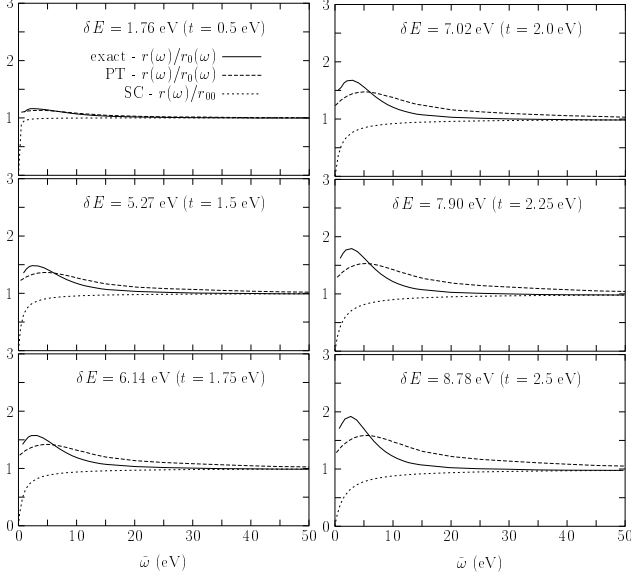


FIG. 6.  $r(\omega)/r_0(\omega)$  from the semi-classical approximation (SC), the first order perturbation expansion (PT) as well as the exact time evolution calculations for different values of the excitation energy  $\delta E$  and for  $U/t = 5.76$ . The remaining parameters are taken from  $\text{CuCl}_2$  ( $R_0^{\text{Cl}} = 4.71$  a.u.).

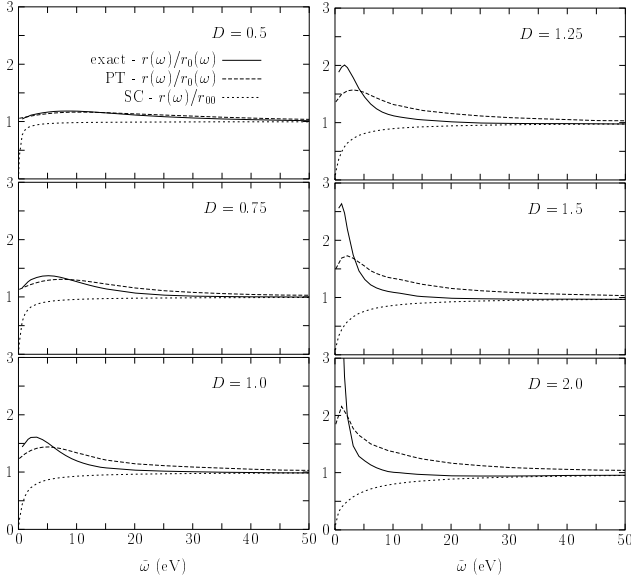


FIG. 7. The same as in Fig. 6 but varying the range  $DR_0$  instead of  $\delta E$ , where  $D$  is a scale factor. The parameters of  $\text{CuCl}_2$  are used.

In Figs. 6 and 7 we compare the perturbation expansion with the exact time dependent calculation for a realistic scattering potential in the symmetric case. In the symmetric case we have  $\delta E = 2t\sqrt{1+r_{00}} =$

$(U/2)\sqrt{1+1/r_{00}}$ , and  $U = -V_{sc}(0)$ . Since the ratio  $r_0(\omega)$  was discussed extensively in Sec. IV, we here focus on  $r(\omega)/r_0(\omega)$ , which describes the effect of the scattering potential. We vary the excitation energy  $\delta E$  by varying  $t$ , while keeping  $r_{00}$  constant. We also vary the potential range by replacing  $R_0$  in Eq. (11) by  $DR_0$  and then varying  $D$ . With  $r_{00}$  fixed,  $\delta E$  is proportional to  $V_{sc}(0)$ . Thus a small  $\delta E$  and a small  $D$  make the perturbation weak. The calculations are made for a range of parameter values around those given for  $\text{CuCl}_2$  in Table II.

## B. Semi-classical approach

We can also perform the photoemission calculation by assuming a classical trajectory of the emitted photoelectron<sup>25</sup>, producing a time-dependent potential which drives the dynamics of the the model. It has been reported that the semi-classical approach can give the unexpectedly good results for the systems with coupling to plasmons.<sup>4,19,26</sup> The essence of the semi-classical approach is to replace the scattering potential  $V_{sc}(r)$  by a time-dependent potential using the charge density  $\rho(\mathbf{r}, \tau)$  of the emitted electron, *i.e.*

$$V_{sc}(r) \rightarrow \int d\mathbf{r} V_{sc}(r) \rho(\mathbf{r}, \tau) = V_{sc}(v\tau), \quad (70)$$

where we have used  $\rho(\mathbf{r}, \tau) = \delta(\mathbf{r} - \mathbf{v}\tau)$ . We can then write the Hamiltonian as

$$\mathcal{H}(\tau) = \mathcal{H}_0(n_c = 0) + V(\tau), \quad (71)$$

where  $\mathcal{H}_0(n_c = 0)$  can be expressed in terms of the exact final states ( $\psi_1$  and  $\psi_2$ ) in the presence of a core hole

$$\mathcal{H}_0(n_c = 0) = E_1 \psi_1^\dagger \psi_1 + E_2 \psi_2^\dagger \psi_2. \quad (72)$$

The time-dependent potential takes the form

$$\begin{aligned} V(\tau) &= n_b V_{sc}(v\tau) \\ &= V_{11}(\tau) \psi_1^\dagger \psi_1 + V_{22}(\tau) \psi_2^\dagger \psi_2 + V_{12}(\tau) (\psi_1^\dagger \psi_2 + \psi_2^\dagger \psi_1), \end{aligned} \quad (73)$$

where (cf. Eq. (54))

$$\begin{aligned} V_{11}(\tau) &= \sin^2 \varphi V_{sc}(v\tau), & V_{22}(\tau) &= \cos^2 \varphi V_{sc}(v\tau), \\ V_{12}(\tau) &= V_{21}(\tau) = -\frac{1}{2} \sin 2\varphi V_{sc}(v\tau). \end{aligned} \quad (74)$$

The remaining system (target) is still purely quantum mechanical, and we write its time-dependent wave function  $|\Psi(\tau)\rangle$  as

$$|\Psi(\tau)\rangle = a_{1v}(\tau) |\psi_1\rangle e^{-iE_1\tau} + a_{2v}(\tau) |\psi_2\rangle e^{-iE_2\tau}. \quad (75)$$

The classical electron velocity  $v$  is determined by energy conservation, that is,  $\frac{1}{2}v^2 = \tilde{\omega}$ . We have here chosen the velocity corresponding to the satellite. We could also

have performed two calculations, with the velocities corresponding to the leading peak and to the satellite, respectively. In contrast to the approach used here, this would, however, lead to the problem that the spectral weight would not be normalized. Applying the time-dependent Schrödinger equation to  $|\Psi(\tau)\rangle$ , we obtain  $a_{1v}(\tau)$  and  $a_{2v}(\tau)$ ,

$$i\frac{\partial}{\partial\tau}a_{1v}(\tau) = V_{11}(\tau)a_{1v}(\tau) + V_{12}(\tau)a_{2v}(\tau)e^{-i\delta E\tau}, \quad (76)$$

$$i\frac{\partial}{\partial\tau}a_{2v}(\tau) = V_{22}(\tau)a_{2v}(\tau) + V_{21}(\tau)a_{1v}(\tau)e^{i\delta E\tau}, \quad (77)$$

where  $\delta E$  (Eq. (30)) is the optical excitation energy. Eqs. (76) and (77) are subject to the initial conditions (cf Eq. 32)

$$a_{sv}(0) = w_s. \quad (78)$$

The final photoemission currents  $J_i(\omega)$  is

$$J_i(\omega) \propto |a_{iv}(\tau_0)|^2, \quad i = 1, 2. \quad (79)$$

It is sufficient to perform the calculation up to  $\tau = \tau_0 \equiv R_0/v$ , since the potential vanishes for larger values of  $\tau$ . The relative intensity between main and satellite contributions is given by  $r(\omega) = J_2(\omega)/J_1(\omega)$  as before.

In Figs. 6 and 7 we compare the semi-classical and exact results for a realistic potential in the symmetric case. The semi-classical theory is inaccurate over most of the energy range considered here. For large energies however, the semi-classical theory comes much closer to the exact result than does the PT. It is also clear that an increasing  $\delta E$  ( $\simeq V_{sc}(0)$ ) does not noticeably affect the energy for the adiabatic-sudden transition, where it strongly effects the maximum deviation. An increasing  $D$  on the other hand not only strongly increases the maximum deviation, but also makes the adiabatic-sudden transition energy smaller. The dependence on the parameters will be investigated more extensively in the next section.

## VII. ADIABATIC-SUDDEN TRANSITION

We are now in a position to address the adiabatic-sudden transition and its dependence on the parameters. The calculations are performed with the analytical matrix elements in Eqs. (18, 20). First we study the different characteristic lengths,  $\tilde{R}_d$  for the dipole matrix elements, and  $\tilde{R}_s$  and  $\tilde{R}_{sd}$  for the scattering potential matrix elements. We find that it makes sense to use only one effective length  $\tilde{R}$ , and the corresponding energy  $\tilde{E} = 1/(2\tilde{R}^2)$ . As we remarked in Sec. VD,  $r/r_0$  as a function of  $\tilde{\omega}/\tilde{E}$  depends on the parameters  $\delta E/\tilde{E}$  and  $\tilde{V}/\tilde{E}$ , and also on the "system" parameters  $\theta$  and  $\varphi$ . We vary  $\delta E$  independently of  $\tilde{V}$ , although for a given

model there is a direct relation between these two quantities. Part of this relation can be offset by using different  $\theta$  and  $\varphi$  (with  $r_{00}$  constant) but we do not explore this possibility. The exact solution with a separable potential is used to discuss the validity and breakdown of perturbation theory. We find that  $\tilde{V}/\tilde{E}$  has a large effect on the deviation from the sudden limit, but little effect on the value of  $\tilde{\omega}/\tilde{E}$  where the deviation becomes small, while  $\delta E/\tilde{E}$  has a comparatively small effect on both magnitude and range of the deviation. For simplicity we use the  $\text{CuCl}_2$  parameters  $\theta = \varphi = 0.3$ , which gives  $r_{00} = 2.1$ . For  $\text{CuCl}_2$  we further have  $\tilde{V} = -0.36$  a.u.,  $\tilde{E} = 0.195$  a.u. ( $\tilde{R} = 1.6$  a.u.), and  $\delta E = 0.237$  a.u., i.e.,  $\tilde{V}/\tilde{E} = -1.85$  and  $\delta E/\tilde{V} = -0.66$ . In our calculations, we vary  $\tilde{V}/\tilde{E}$  and  $\delta E/\tilde{V}$  by typically a factor of two around these reference values.

### A. Exact numerical treatment with analytic matrix elements

We first illustrate the dependence on the ratio between the length scales  $\tilde{R}_d$ ,  $\tilde{R}_s$ , and  $\tilde{R}_{sd}$ . In Fig. 8 we show the results for different ratios  $\tilde{R}_d/\tilde{R}_s$  keeping  $\tilde{R}_{sd}/\tilde{R}_d = 1$ . These results are obtained for  $\tilde{V}/\tilde{E}_s = -2.0$  and  $\delta E/\tilde{V} = -0.5$ , where  $\tilde{E}_s = 1/(2\tilde{R}_s^2)$  is the energy scale set by the scattering potential length scale. Fig. 8 shows that as  $\tilde{R}_d/\tilde{R}_s$  is reduced the magnitude of the "overshoot" is increased. There are, however, no qualitative changes.

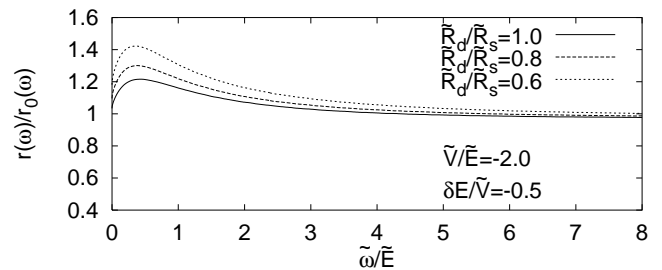


FIG. 8. The ratio  $r(\omega)/r_0(\omega)$  as a function of  $\tilde{R}_d/\tilde{R}_s$  for a fixed  $\tilde{R}_{sd}/\tilde{R}_s = 1$  and for  $\varphi = \theta = 0.3$ . The figure illustrates that there are no qualitative changes as the length scales for the dipole and scattering matrix elements become different.

Fig. 9 shows results for different values of  $\tilde{R}_{sd}/\tilde{R}_s$  for a fixed  $\tilde{R}_d/\tilde{R}_s = 1$ . From Eq. (20) it can be seen that this corresponds to varying the range of values  $k - k'$  where  $V_{kk'}$  is large, without changing the range over which  $V_{kk}$  varies. The figure illustrates that the overshoot becomes larger as  $\tilde{R}_{sd}/\tilde{R}_s$  is reduced. This is natural, since decreasing  $\tilde{R}_{sd}$  effectively makes the scattering potential stronger by expanding the range of values  $k - k'$  with large scattering matrix elements. The qualitative behaviour, however, is not changed. In view of Figs.

8 and 9, we study below the case when  $\tilde{R}_{sd} = \tilde{R}_s = \tilde{R}_d$ , as mentioned in Sec. VD.

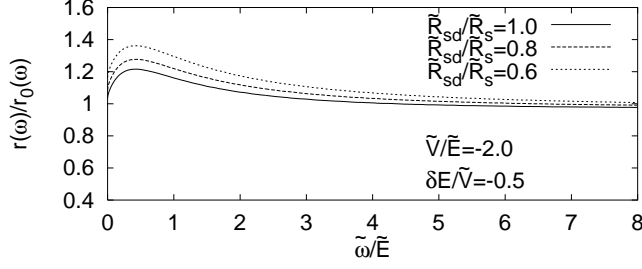


FIG. 9. The ratio  $r(\omega)/r_0(\omega)$  as a function of  $\tilde{R}_{sd}/\tilde{R}_s$  for a fixed  $\tilde{R}_d/\tilde{R}_s = 1$  and for  $\varphi = \theta = 0.3$ . The figure illustrates that there is no qualitative changes as the ratio of the two length scales in the scattering matrix elements is varied.

Fig. 10 shows such results for different values of the strength of the scattering potential  $\tilde{V}/\tilde{E}$  and for different values of the excitation energy  $\delta E/\tilde{V}$ . In each panel  $\delta E/\tilde{V}$  is kept fixed, but the ratio is varied by a factor of four from Fig. 10a to Fig. 10c. Typically  $r(\omega)/r_0(\omega)$  has an overshoot for small values of  $\tilde{\omega}$ . For somewhat larger  $\omega$  the ratio approaches unity and possibly becomes smaller than unity. The overshoot can be fairly large and happens on a small energy scale ( $\sim \tilde{E}$ ). In a few cases of a large overshoot,  $r(\omega)/r_0(\omega)$  does not become approximately unity until  $\tilde{\omega}$  is several times  $\tilde{E}$ , although the relevant energy scale is still  $\tilde{E}$ . In the case of an undershoot,  $r(\omega)/r_0(\omega)$  approaches unity from below very slowly (energy scale much larger than  $\tilde{E}$ ). The undershoot is, however, relatively small, and if we do not require a high accuracy, we consider the sudden approximation is valid when the overshoot becomes small. This means that as the range of the scattering potential is made larger, the sudden limit is reached at a smaller energy. This is the opposite to what one would expect from the semi-classical theory. The figure illustrates that  $\delta E$  is not the relevant energy scale. Since in each panel we keep  $\delta E/\tilde{V}$  fixed, there is a variation of  $\delta E/\tilde{E}$  by a factor of four. Furthermore there is a variation of  $\delta E/\tilde{V}$  by a factor of four in going from the top to the bottom panel in Fig. 10. There is no corresponding change in the energy for the adiabatic to sudden transition.

## B. Separable potential

It is interesting to study a separable potential, since it is then possible to obtain an analytical solution. This makes it easier to interpret the results. It also allows the study the effects of multiple scattering, i.e. the deviations from first order perturbation theory. Fig. 11 shows results of the exact and first order theory using the same values of  $\delta E/\tilde{V}$  and  $\tilde{V}/\tilde{E}$  as in Fig. 10b. The separable potential overestimates the magnitude of the overshoot

in  $r(\omega)/r_0(\omega)$  quite substantially. Otherwise the results are rather similar. For a qualitative discussion, we can therefore use the separable potential.

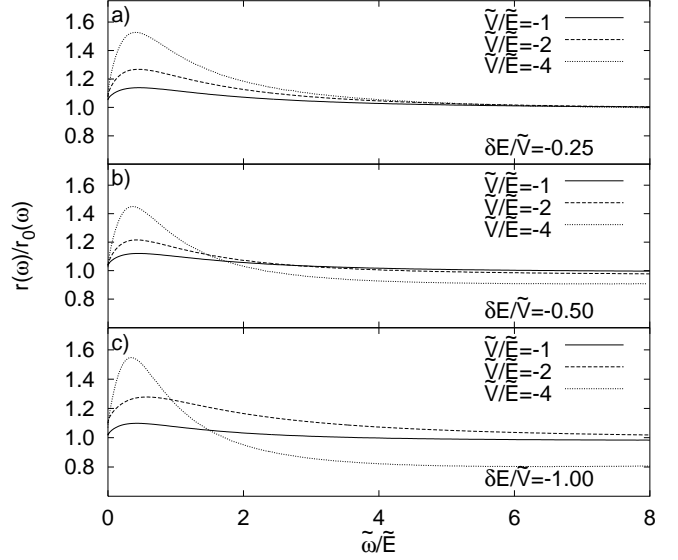


FIG. 10. The ratio  $r(\omega)/r_0(\omega)$  as a function of  $\tilde{\omega}/\tilde{E}$  for different values of  $\tilde{V}/\tilde{E}$  and  $\delta E/\tilde{V}$  and for  $\varphi = \theta = 0.3$ . The figure illustrates that  $\tilde{E}$  is an appropriate energy scale for the adiabatic to sudden transition.

For simplicity, we consider  $\delta E = 0$ . We further put  $M_k = (\tilde{R}k)^2 / [1 + (\tilde{R}k)^3] = b_k$ . This is a poor approximation for large  $k$ , but then anyhow also  $V_{kk'}$  is poorly represented by the separable potential. Our approximations lead to simple results for the functions  $C$ ,  $D$  and  $E$  entering in Eqs. (62-66).

$$C(\epsilon) = -\tilde{E} \sum_{k'} \frac{b_{k'}^2}{\epsilon - \epsilon_{k'} + i\eta} \quad (80)$$

and  $E(\epsilon) = \cos\theta \tilde{M} C(\epsilon)$ . Then

$$D(\epsilon) = -\cos\theta \frac{\tilde{V}}{\tilde{E}} \frac{C(\epsilon)}{1 + (\tilde{V}/\tilde{E})C(\epsilon)}. \quad (81)$$

Since  $D_k$  is independent of  $k$  in this approximation, we have dropped the index  $k$ . The function  $C(\epsilon)$  is shown in Fig. 12. For  $\varphi = \theta$  we can then write

$$\frac{r(\omega)}{r_0(\omega)} = \left| \frac{1 - \frac{\cos^2\varphi}{\cos 2\varphi} \frac{\tilde{V}}{\tilde{E}} C(\tilde{\omega}) / [1 + \frac{\tilde{V}}{\tilde{E}} C(\tilde{\omega})]}{1 - \frac{1}{2} \frac{\tilde{V}}{\tilde{E}} C(\tilde{\omega}) / [1 + \frac{\tilde{V}}{\tilde{E}} C(\tilde{\omega})]} \right|^2. \quad (82)$$

For a level ordering as indicated in Fig. 1,  $0 < \varphi < \pi/4$  and  $\cos^2\varphi/\cos(2\varphi) \geq 1$ . In our standard case with  $\varphi = 0.3$ ,  $\cos^2\varphi/\cos(2\varphi) = 1.11$ . Thus the term in the numerator of Eq. (82) dominates. The factor  $1 + (\tilde{V}/\tilde{E})C(\tilde{\omega})$  gives the multiple scattering, which is not included in the first order perturbation theory, i.e. the first order result is

$$\left[ \frac{r(\omega)}{r_0(\omega)} \right]_{\text{PT}} = \left| \frac{1 - \frac{\cos^2 \varphi}{\cos 2\varphi} \frac{\tilde{V}}{E} C(\tilde{\omega})}{1 - \frac{1}{2} \frac{\tilde{V}}{E} C(\tilde{\omega})} \right|^2. \quad (83)$$

We now compare the behaviors of Eqs. (82) and (83), to see the effects of using perturbation theory. For small values of  $\tilde{\omega}$ ,  $\text{Re}C(\tilde{\omega})$  is positive and then changes sign at about  $\tilde{\omega}/\tilde{E} \sim 2$ .  $\text{Im}C(\tilde{\omega})$  is always positive. Due to our crude approximations for  $b_k$  and  $M_k$ ,  $C(\tilde{\omega})$  rapidly becomes unreliable beyond  $\tilde{\omega}/\tilde{E} = 2$ . Both for the exact and perturbative expressions  $r/r_0$  goes from over- to undershoot approximately when  $\text{Re}C(\tilde{\omega}) = 0$ . This is somewhat earlier than in Fig. 11, where however  $\delta E = 0.5$ . Comparing  $r(\omega)/r_0(\omega)$  for the exact (Eq. (82)) and the first order result (Eq. (83)), we find that the exact solution is larger when  $\text{Re}C(\tilde{\omega}) \gtrsim \text{Im}C(\tilde{\omega})$ , cf Fig. 11. This is consistent with second order perturbation theory, which is found to enhance  $r(\omega)/r_0(\omega)$  for small  $\tilde{\omega}$  and reduce it for large  $\tilde{\omega}$ . For  $\tilde{\omega} = 0$ ,  $C(\tilde{\omega})$  is purely real and slightly larger than 0.1, thus multiple scattering gives a divergence in both  $J_1(\tilde{\omega})$  and  $J_2(\tilde{\omega})$  when  $\tilde{V}/\tilde{E} \sim -10$ . This is due to the attractive potential  $V$  forming a bound state from the continuum states.

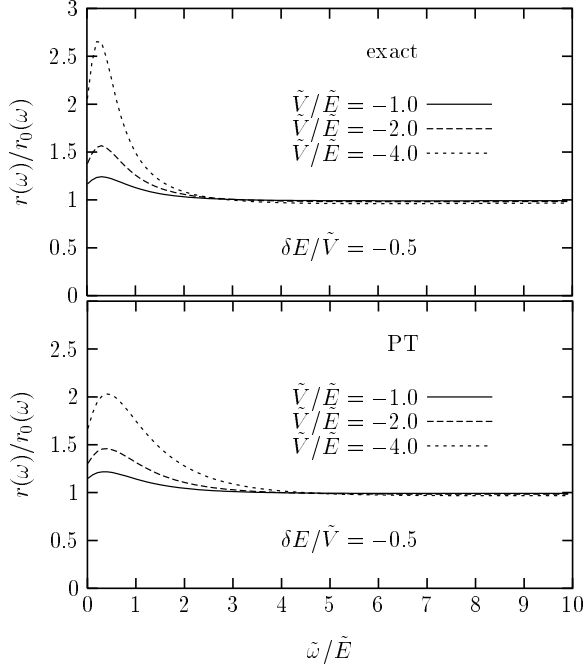


FIG. 11. The ratio  $r(\omega)/r_0(\omega)$  for a separable scattering potential (57). According to the exact result in upper panel, the overshoot is substantially overestimated by the separable potential compared to Fig. 10b, but there is still a qualitative agreement with the more realistic model (20). The lower panel shows how perturbation theory works and it illustrates the effects of multiple scattering.

The important conclusion from analysing the separable potential is that if  $\tilde{V}$  is not too large, first order perturbation theory gives roughly the correct range over which

there are essential deviations from the sudden limit, while multiple scattering increases the magnitude of these deviations for small  $\tilde{\omega}$  and slightly decreases them for larger  $\tilde{\omega}$ .

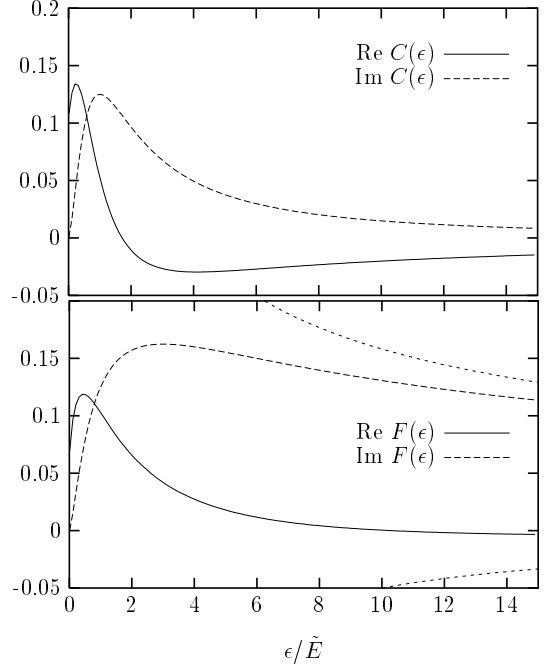


FIG. 12. The function  $C(\epsilon)$  relevant for a separable potential is given in the upper panel. The low panel gives the behaviors of  $F(\epsilon)$  defined in Eq.(84). The dotted lines give the asymptotic behaviors of  $F(\epsilon)$  in Eq.(88).

We next discuss the physical interpretation of the expression (82) (or the perturbational expressions in (67, 68, 69)). Here unity (the first term in (67, 68, 69)) corresponds to a direct transition into the final continuum state corresponding to energy conservation. The second term (the last two terms in (67, 68, 69)) corresponds to a virtual transition into some other continuum state followed by one or several scattering events with the electron ending up in the continuum state corresponding to energy conservation. Let us consider the virtual emission into a continuum state with a larger energy than the final state and let this be followed by one scattering event into the final state. For a negative  $\tilde{V}$  the interference with the direct event is then constructive. For small photon energies such events dominate for two reasons. Firstly, there are many more states available above the energy corresponding to energy conservation than below, and secondly the dipole matrix elements suppress the transitions to the energies below. As a result, both the main peak and the satellite are enhanced by the scattering effects. For the values of  $\varphi$  and  $\theta$  considered here ( $< \pi/4$ ), the relative effect is stronger for the satellite. As a result  $r(\omega)/r_0(\omega)$  is enhanced. For larger photon energies  $\text{Re}C(\tilde{\omega})$  becomes negative. The density of states of par-

tial waves with given  $l$  and  $m$  quantum numbers decreases with energy ( $\sim 1/\sqrt{\epsilon}$ ). This favours virtual emissions to states below the final continuum state. Depending on the model for  $b_k$  and  $M_k$ , these matrix elements may have the same effect. As a result,  $\text{Re } C(\tilde{\omega})$  becomes slightly negative for large energies and the ratio  $r(\omega)/r_0(\omega)$  is slightly smaller than one.

The relevant energy scale for  $C(\omega)$  is  $\tilde{E}$ . This is a combination of the two effects discussed above. The turn on of the dipole matrix elements on an energy scale of the order  $\tilde{E}$  favors an increasing value of  $C$  over this energy scale, while the density of states effects becomes more important for larger energies. As a result, both  $\text{Re } C(\omega)$  and  $\text{Im } C(\omega)$  have a maximum at an energy of the order  $\tilde{E}$ .

### C. Perturbational treatment with analytic matrix elements

In this section we study the perturbation theory expression in more detail and without relying on a separable potential. Instead we consider the more realistic matrix elements in Eqs. (18) and (20), assuming that  $\tilde{R}_d = \tilde{R}_s = \tilde{R}_{sd} = \tilde{R}$ . We define a function  $F_k$  by

$$\sum_{k'} \frac{V_{kk'} M_{k'}}{\epsilon - \epsilon_{k'} + i\eta} \equiv -\frac{\tilde{V}}{\tilde{E}} M_k F_k(\epsilon/\tilde{E}), \quad (84)$$

which is possible due to the simple form of  $V_{kk'}$  and  $M_{k'}$ . Explicitly we have

$$F_k(\epsilon) = \frac{1}{\pi} \int_0^\infty \frac{x^4 dx}{[1+x^2]^2 \left[1 + (\tilde{R}k - x)^2\right] [x^2 - \epsilon - i\eta]}. \quad (85)$$

From Eqs. 68 and 69 we have

$$\frac{r(\omega)}{r_0(\omega)} = \left| \frac{1 - \cos^2 \varphi \frac{\tilde{V}}{\tilde{E}} F_{k_2} \left(\frac{\tilde{\omega}}{\tilde{E}}\right) - \frac{\sin 2\varphi \sin(\varphi+\theta)}{2 \cos(\varphi+\theta)} \frac{\tilde{V}}{\tilde{E}} F_{k_2} \left(\frac{\tilde{\omega}+\delta E}{\tilde{E}}\right)}{1 - \sin^2 \varphi \frac{\tilde{V}}{\tilde{E}} F_{k_1} \left(\frac{\tilde{\omega}+\delta E}{\tilde{E}}\right) - \frac{\sin 2\varphi \cos(\varphi+\theta)}{2 \sin(\varphi+\theta)} \frac{\tilde{V}}{\tilde{E}} F_{k_1} \left(\frac{\tilde{\omega}}{\tilde{E}}\right)} \right|^2. \quad (86)$$

Since  $\tilde{R}k_2 = \sqrt{\tilde{\omega}/\tilde{E}}$  and  $\tilde{R}k_1 = \sqrt{(\tilde{\omega} + \delta E)/\tilde{E}}$  we see, as stated earlier, that  $r/r_0$  depends only on  $\tilde{V}/\tilde{E}$ ,  $\delta E/\tilde{E}$  and  $\tilde{\omega}/\tilde{E}$ .

First we consider the limit of small values of  $k$  and  $\delta E$ . For  $\tilde{\omega} = \delta E = 0$  we have  $F_0(0) = 1/16$ , and

$$\frac{r(0)}{r_0(0)} = \left[ \frac{1 + \frac{|\tilde{V}|}{\tilde{E}} \cos \varphi \cos \theta / (16 \cos(\varphi + \theta))}{1 + \frac{|\tilde{V}|}{\tilde{E}} \sin \varphi \cos \theta / (16 \sin(\varphi + \theta))} \right]^2. \quad (87)$$

If the more localized level  $a$  is above  $b$  (see Fig. 1) in the initial state and below  $b$  in the final state ("shake-down"), we have  $0 < \varphi < \pi/4$  and  $0 < \theta < \pi/4$ , and the factor in the brackets is larger than unity. Thus interaction effects enhance the ratio  $r(\omega)/r_0(\omega)$ . This corresponds to a constructive interference between intrinsic and extrinsic effects. This is in contrast to the destructive interference found for the plasmon case.<sup>4,5</sup> The present treatment, however, refers to the "shake-down" scenario, and it is more appropriate to compare the plasmon case with the "shake up" case ( $-\pi/4 < \varphi < 0 < \theta < \pi/4$  and  $\varphi + \theta < 0$ ). Then the expression (87) for  $r(\omega)/r_0(\omega)$  indeed becomes smaller than one, and the relative weight of the satellite is reduced for small energies. We notice, however, that both the satellite and the main peak are enhanced by the interference, but that the main peak is enhanced more in the "shake-up" situation.

We next consider the case when  $k$  is large.  $F_k(\epsilon)$  for large  $k$  and  $\epsilon$  is (with  $\tilde{R}k \approx \sqrt{\epsilon}$ )

$$F_k(\epsilon) = \frac{1}{2\sqrt{\epsilon}} \left[ i - \frac{1}{2\sqrt{\epsilon}} + \tilde{R}k - \sqrt{\epsilon} \right]. \quad (88)$$

For the case when  $\theta = \varphi$  we obtain

$$\frac{r(\omega)}{r_0(\omega)} - 1 = -\frac{|\tilde{V}|}{2\tilde{\omega}} \frac{1 + \delta E/\tilde{E}}{2 \cos(2\varphi)} + \frac{|\tilde{V}|^2}{4\tilde{\omega}\tilde{E}} \left( \frac{\cos^4 \varphi}{\cos^2(2\varphi)} - \frac{1}{4} \right). \quad (89)$$

Thus the approach to the sudden limit goes as  $1/\tilde{\omega}$  with a coefficient which depends on the parameters. With our standard  $\text{CuCl}_2$  parameters, we have

$$\frac{r(\omega)}{r_0(\omega)} - 1 = -0.30 \frac{|\tilde{V}|}{\tilde{\omega}} \left( 1 + \frac{\delta E}{\tilde{E}} \right) + 0.24 \frac{|\tilde{V}|^2}{\tilde{\omega}\tilde{E}}$$

We note that for large  $|\tilde{V}|/\tilde{E}$ , and when  $|\tilde{V}|$  is large enough compared to  $\delta E$ , the last (positive) term dominates. The approach to the sudden limit is then set by  $|\tilde{V}|^2/\tilde{E} = 2 \left( \tilde{R}\tilde{V} \right)^2$ .

To evaluate Eq.(86) when  $\delta E = 0$  we only need the function  $F(\epsilon)$ ,

$$F(\epsilon) = \frac{1}{\pi} \int_0^\infty \frac{x^4 dx}{[1+x^2]^2 \left[1 + (\sqrt{\epsilon} - x)^2\right] [x^2 - \epsilon - i\eta]}.$$

We show  $F(\epsilon)$  in the lower panel of Fig.12. The results Eq. (88) for large values of  $\epsilon$  are shown by the dotted lines in the figure. Clearly the approach of  $\text{Re } F$  to its asymptote is very slow. If we take  $\delta E = 0$  we have the same form as in first order perturbation theory with a separable potential Eq. (83),

$$\frac{r(\omega)}{r_0(\omega)} = \left| \frac{1 - \frac{\cos^2 \varphi}{\cos 2\varphi} \frac{\tilde{V}}{\tilde{E}} F(\tilde{\omega})}{1 - \frac{1}{2} \frac{\tilde{V}}{\tilde{E}} F(\tilde{\omega})} \right|^2, \quad (90)$$

where we have put  $\varphi = \theta$ . As shown in Fig. 12,  $F(\epsilon)$  has a qualitatively similar behavior as  $C(\epsilon)$  for  $\epsilon/\tilde{E} \lesssim 2$ . As in the case of the function  $C$ , the relevant energy scale is  $\tilde{E}$ .

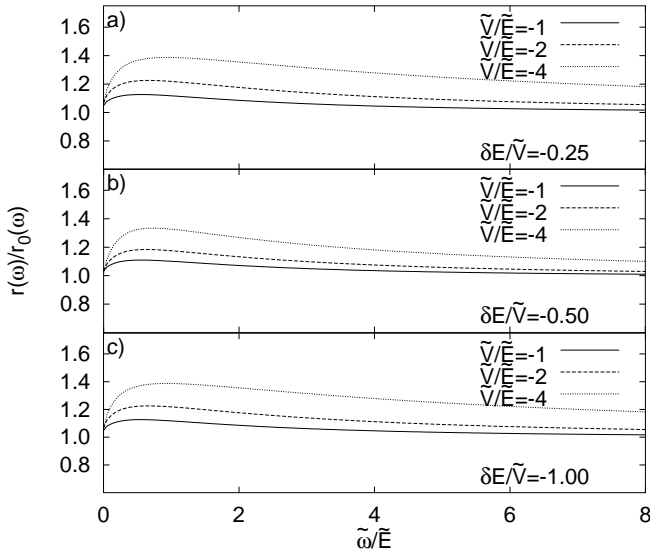


FIG. 13. The ratio  $r(\omega)/r_0(\omega)$  as a function of  $\tilde{\omega}/\tilde{E}$  for different values of  $\tilde{V}/\tilde{E}$  and  $\delta E/\tilde{V}$ .

In Fig. 13 we show  $r(\omega)/r_0(\omega)$  as a function of  $\tilde{\omega}/\tilde{E}$  for a few values of  $\delta E/\tilde{V}$  and  $\tilde{V}/\tilde{E}$ . We see that  $r(\omega)/r_0(\omega)$  starts at a positive value (cf Eq. (87)), and reaches a broad maximum at about  $\tilde{\omega}/\tilde{E} \sim 0.5 - 1.5$ . Compared to the separable potential solution in Fig. 11, the overshoot behavior is robust up to fairly large energies, which is due to  $\text{Im}F(\tilde{\omega})$  decaying more slowly than  $\text{Im}C(\tilde{\omega})$ . For much larger values of  $\omega$ ,  $(r/r_0 - 1)$  decays as  $1/\tilde{\omega}$ , as shown in Eq. (89). Here, based on the discussion in Sec. VIIB, we can expect that as multiple scattering becomes important, the region where there is an overshoot is substantially reduced and the region with an undershoot becomes larger. At the same time, the overshoot intensity will be enhanced. These behaviors are actually confirmed by comparing with the exact calculations given in Fig. 10.

Fig. 13 illustrates that for intermediate values of  $\tilde{\omega}$ , when  $\text{Re}F$  dominates,  $(r/r_0 - 1)$  goes as roughly  $|\tilde{V}|/\tilde{\omega}$  if  $\delta E/\tilde{E}$  is not too large. For larger (but not too large) values of  $\tilde{\omega}$ ,  $\text{Re}F$  becomes small and  $\text{Im}F$  dominates. Since  $\text{Re}F$  is positive for small energies, this leads to a constructive interference between intrinsic and extrinsic effects. For energies of the order  $\tilde{E}$ ,  $\text{Re}F$  changes sign, and the interference becomes weakly destructive. For somewhat larger energies the extrinsic effects are mainly determined by the imaginary part of  $F$ . From Eq. (89) it follows that in perturbation theory the extrinsic effects become small on the energy scale  $\tilde{V}^2/\tilde{E}$ .

#### D. Semi-classical approximation

In this section we analyze the adiabatic-sudden transition within the semi-classical framework. From the coupled differential equations Eqs. (76) and (77) we can obtain differential equations for  $\partial|a_{iv}(\tau)|^2/\partial\tau$ ,  $i = 1, 2$ . Integration of these equations, leads to

$$\begin{aligned} & |a_{2v}(\tau_0)|^2 - |a_{2v}(0)|^2 \\ &= 2\text{Im} \int_0^{\tau_0} V_{12}(\tau) a_{1v}(\tau) a_{2v}^*(\tau) e^{i\delta E\tau} d\tau, \end{aligned} \quad (91)$$

where  $\tau_0 = R_0/v$  is the time at which the emitted electron with the velocity  $v$  leaves the range  $R_0$  of the scattering potential.  $|a_{iv}(\tau_0)|^2 - |a_{iv}(0)|^2$  is a measure of the deviation from the sudden limit. For small values of  $\tau$  both the coefficients  $a_{iv}(\tau)$  and the exponent  $e^{i\delta E\tau}$  are approximately real and there is a small contribution to the imaginary part of the integral in Eq. (91). As  $\tau$  grows there is, however, a contribution from both these sources.

To obtain a qualitative understanding of the semi-classical approximation, we solve the Schrödinger equations Eqs. (76) and (77) to lowest order in  $1/v$ . This leads to

$$\begin{aligned} a_{1v}(\tau) &= a_{1v}(0) \\ &- i \int_0^\tau d\tau' [V_{11}(\tau') a_{1v}(0) + V_{12}(\tau') a_{2v}(0)] \end{aligned} \quad (92)$$

and a similar result for  $a_{2v}(\tau)$ . This gives

$$\begin{aligned} |a_{2v}(\tau_0)|^2 - |a_{2v}(0)|^2 &= \frac{1}{2} \sin(2\varphi) \left\{ \frac{1}{2} \sin(2\theta) \right. \\ &\times \left[ \int_0^{\tau_0} d\tau V_{sc}(\tau) \right]^2 + \sin(2\varphi + 2\theta) \delta E \int_0^{\tau_0} d\tau \tau V_{sc}(\tau) \left. \right\}. \end{aligned} \quad (93)$$

To discuss the result, we for a moment assume a simple  $\tau$ -dependence of  $V_{ij}(\tau)$

$$V_{ij}(\tau) = V_{ij}(0) \left(1 - \frac{\tau}{\tau_0}\right), \quad (94)$$

which corresponds to the  $r$ -dependence used in Eq. (22). We note, however, that this form is too simple to describe the behavior of the more realistic potential in Eq. (11). Inserting Eqs. (92) and (94) in Eq. (93) gives

$$\begin{aligned} \Delta_2 \equiv |a_{2v}(\tau_0)|^2 - |a_{2v}(0)|^2 &= \frac{1}{4} V_{sc}(0) \sin(2\varphi) \\ &\times \left[ \frac{1}{4} \sin(2\theta) V_{sc}(0) + \frac{1}{3} \sin(2\varphi + 2\theta) \delta E \right] \tau_0^2. \end{aligned} \quad (95)$$

We now extend this treatment to intermediate values of  $v$  where the adiabatic to sudden transition takes place. Using the expressions Eqs. (25), (28) and (30) to relate  $\delta E$  and  $U = -V_{sc}(0)$  we obtain



$$\frac{r(\omega)}{r_0} - 1 = \frac{\Delta_2}{\sin^2(2\varphi) \cos^2(2\varphi)} = -\frac{\sin(2\varphi)}{\sin(2\theta)} \frac{(\delta E)^2 \tau_0^2}{12}. \quad (96)$$

Within the semi-classical theory the condition for the sudden approximation is then

$$\frac{v}{R_0} = \frac{1}{\tau_0} \gg \delta E \sqrt{\frac{\sin(2\varphi)}{12 \sin(2\theta)}}. \quad (97)$$

We are now in a position to discuss the approach to the sudden limit. Within a semi-classical framework it seems clear that we have to require that the hole potential is fully switched on after a “short” time  $\tau_0 = v/R_0$ , i.e., that the emitted electron leaves the range of the scattering potential after a short time. The question is, however, what we mean by “short”. From Eq. (95) it follows that the time-scale is set by both the inverse of  $\delta E$  and the inverse of  $V_{sc}(0)$ . In Eq. (97) we have used the relation between  $\delta E$  and  $V_{sc}(0)$  to remove  $V_{sc}(0)$  from Eq. (97).

From Eq. (97) we obtain the condition for the sudden approximation within the SC theory

$$\tilde{\omega} = \frac{1}{2} k^2 \gg (\delta E)^2 R_0^2 = \frac{(\delta E)^2}{2\tilde{E}} \sim \frac{V_{sc}(0)^2}{\tilde{E}}. \quad (98)$$

Thus, according to the semi-classical theory, the sudden approximation requires that  $\epsilon_k \gg (\delta E)^2/\tilde{E}$ . Comparison with the full quantum mechanical calculations in Fig. 10 shows that this criterion is not appropriate for the range of parameters considered here. The reason is that we have considered a parameter range where the semi-classical theory is not very accurate.

It is interesting that the SC theory correctly predicts that the weight of the satellite goes to zero at threshold. Nevertheless, the SC theory does not give the correct physics at the threshold. In the full quantum mechanical calculation the weight of the satellite goes to zero due to the effects of the dipole matrix element, which becomes very small at small photoelectron energies. This effect is not included in the SC theory. In the semi-classical treatment, the small weight of the satellite is due to the fact that the scattering potential between the outgoing slow electron and the excitation means that the hole potential is only switched on slowly. In the quantum mechanical treatment, on the other hand, the scattering potential leads to an enhancement of the relative weight of the satellite close to the threshold for the shake-down case.

### VIII. DISCUSSION

We have studied the photoemission spectrum of a simple model with a localized charge transfer excitation. We have obtained exact numerical results for the spectrum as a function of the photon energy  $\omega$  and in particular focussed on the ratio  $r(\omega)$  between the weights of the

satellite and the main peak. These calculations are compared with perturbational and semi-classical treatments. The results have been analyzed using the latter two approaches.

An important effect in the ratio  $r(\omega)$  is due to the energy dependence of the dipole matrix elements and a factor  $1/(\partial\epsilon_k/\partial k) \sim 1/k$  in the expression for the spectrum. This leads to a suppression of the satellite close to the threshold, but can lead to an overshoot further away from the threshold. This effect was discussed in Sec. IV and is described by  $r_0(\omega)$ . If the interaction between the emitted electron and the target is weak, this effect dominates. It is determined by the excitation energy  $\delta E$  and the relevant energy scale  $\tilde{E}_d$  of the dipole matrix element. If  $\delta E/\tilde{E}_d$  is small,  $r_0$  reaches its limiting value from below, while there is an overshoot if  $\delta E/\tilde{E}_d \gg 1$ . In both cases  $r_0$  reaches its limiting value for a kinetic energy of the order a few times  $\delta E$ .

To study the effects of the scattering potential between the emitted electron and the target we have focussed on the ratio  $r(\omega)/r_0(\omega)$ . This quantity shows an overshoot for small values of  $\omega$  in the “shake-down” situation studied here. Depending on the parameters there may be an undershoot for larger energies, which extends over a large energy range. This undershoot is, however, fairly small for the cases considered here. The sudden approximation is then valid to a reasonable accuracy when the overshoot has become small. We show that this happens on the energy scale  $\tilde{E} = 1/(2\tilde{R}^2)$ , where  $\tilde{R}$  is a typical length scale of the scattering potential.

One of the main results of this paper is that for a coupling to localized excitations, the adiabatic to sudden transition takes place at quite small kinetic energies of the photoelectron. This is in contrast to the large kinetic energies needed for the case of coupling to plasmons. In the plasmon case, the kinetic energy is typically so large that the semi-classical treatment is a very good approximation. The adiabatic to sudden transition is then expected to happen on the energy scale  $(\omega_q \lambda)^2$ ,<sup>19</sup> where  $\omega_q$  and  $\lambda$  are the plasmon frequency and wavelength, respectively. Since the long wavelength plasmons dominate the transition, this happens at very large energies. For a localized excitation, the relevant length scale of the scattering potential is smaller, and the transition is expected to take place at a smaller energy scale. Actually, the transition takes place at such a small energy that the semi-classical theory is usually not valid any more. It is interesting that the semi-classical theory therefore predicts the opposite dependence on the range  $\tilde{R}$  of the scattering potential, namely as  $\tilde{R}^2$  instead of  $\tilde{E} = 1/(2\tilde{R}^2)$ .

For the “shake-down” scenario considered here (the two outer levels cross as the hole is created), we find constructive interference (increase of  $r(\omega)/r_0(\omega)$ ) between the intrinsic and extrinsic processes at low photoelectron energies. This is in contrast to the destructive interference found in the plasmon case and to the reduction of  $r(\omega)/r_0(\omega)$  found here for the “shake-up” case (no level

crossing).

## ACKNOWLEDGEMENT

This work has been supported by the Max-Planck Forschungspreis. One of us (LH) carried out part of his contribution to this work at the Max-Planck Institute for Festkörperforschung.

- 
- <sup>1</sup> C.-O. Almbladh and L. Hedin in *Handbook on Synchrotron Radiation*, Vol. **1B**, ed. E.-E. Koch, North-Holland Pub. Co. (1983).
- <sup>2</sup> W.L. Schaich and N.W. Ashcroft, Phys. Rev. B **3**, 2452 (1971).
- <sup>3</sup> C.N. Berglund and W.E. Spicer, Phys. Rev. **136**, A1030 (1964); J.J. Chang and D.C. Langreth, Phys. Rev. B **5**, 3512 (1972); *ibid* **8**, 4638 (1973); C. Caroli, D. Lederer-Rosenblatt, B. Roulet, and D. Saint-James, Phys. Rev. B **8**, 4552 (1993); A.C. Simonsen, F. Yubero, and S. Tougaard, Phys. Rev. B **56**, 1612 (1997).
- <sup>4</sup> L. Hedin, J. Michiels, and J. Inglesfield, Phys. Rev. B **58**, 15 565 (1998).
- <sup>5</sup> J.E. Inglesfield, Solid State Commun. **40**, 467 (1981).
- <sup>6</sup> J.C. Fuggle, R. Lässer, O. Gunnarsson, and K. Schönhammer, Phys. Rev. Lett. **44**, 1090 (1980).
- <sup>7</sup> F. Wuilleumier and M. O. Krause, Phys. Rev. A **10**, 242 (1974).
- <sup>8</sup> D. A. Shirley, U. Becker, P. A. Heimann, and B. Langer, Journ. de Physique C9,427 (1987).
- <sup>9</sup> A. Kotani and Y. Toyozawa, J. Phys. Soc. Japan, **37**, 912 (1974).
- <sup>10</sup> O. Gunnarsson and K. Schönhammer, Phys. Rev. Lett. **50**, 604 (1983); Phys. Rev. B **28**, 4315 (1983).
- <sup>11</sup> K. Schönhammer and O. Gunnarsson, Solid State Commun. **23**, 691 (1997); **26**, 399 (1978); O. Gunnarsson and K. Schönhammer, Phys. Rev. Lett. **78**, 1608 (1978).
- <sup>12</sup> J. Fuggle, E. Umbach, D. Menzel, K. Wandelt, and C. Brundle, Solid. State Commun. **27**, 65 (1978).
- <sup>13</sup> S. Larsson, Chem. Phys. Lett. **40**, 362 (1976); S. Larsson and M. Braga, Chem. Phys. Lett. **48**, 596 (1977).
- <sup>14</sup> B. Wallbank, I.G. Main, and C.E. Johnson, J. Electron Spectrosc. Relat. Phenom. **5**, 259 (1974).
- <sup>15</sup> G. van der Laan, C. Westra, C. Haas, and G.A. Sawatzky, Phys. Rev. B **23**, 4369 (1981).

- <sup>16</sup> D.K.G. de Boer, C. Haas, and G.A. Sawatzky, Phys. Rev. B **29**, 4401 (1984).
- <sup>17</sup> A. Fujimori, F. Minami, and S. Sugano, Phys. Rev. B **29**, 5225 (1984); A. Fujimori and F. Minami, Phys. Rev. B **30**, 957 (1984).
- <sup>18</sup> M.A. van Veenendaal, H. Eskes, and G.A. Sawatzky, Phys. Rev. B **47**, 11642 (1993).
- <sup>19</sup> J.E. Inglesfield, J. Phys. C: Solid State Phys. **16**, 403 (1983).
- <sup>20</sup> M. Kaupp, private communications; for example, in the atomic configuration of the Cu-Cl octahedral cluster in CuCl<sub>2</sub>,  $l_c = 5.59$  a.u.,  $l_a = l_b = 4.27$  a.u., and the average distance of them will  $R_0 = 4.71$  a.u. (see the inset of Fig.2a).
- <sup>21</sup> J.C. Slater, Phys. Rev. **36**, 57 (1930).
- <sup>22</sup> J.J. Yeh and I. Lindau, At. Data Nucl. Data Tables **32**, 1(1985).
- <sup>23</sup> A solution of the time-dependent Schrödinger equation was also used in O. Gunnarsson and K. Schönhammer, Phys. Rev. B **31**, 4815 (1985).
- <sup>24</sup> O. Gunnarsson and K. Schönhammer, Phys. Rev. B **22**, 3710 (1980).
- <sup>25</sup> G.D. Mahan, Phys. Status Solidi b **55**, 703 (1973); A.M. Bradshaw, W. Domcke, and L.S. Cederbaum, Phys. Rev. B **16**, 1480 (1977).
- <sup>26</sup> W. Bardyszewski and L. Hedin, Physica Scripta, **32**, 439 (1985).

TABLE I. The model Hamiltonian Eq.(1) can describe various charge transfer systems. The table indicates the meaning of the states  $a$  and  $b$  for different cases.

	a	b
transition metal compounds	$3d$ state	ligand state
CO on surface	$2\pi^*$ state	bulk(surface) state
Ce compounds	$4f$ state	$5d$ state

TABLE II. Used parameters for copper-dihalide compounds.

	$U$ (eV)	$t$ (eV)	$\delta E$ (eV)	$R_0$ (a.u.)	$\epsilon$	$r(\omega \rightarrow \infty)$
CuBr <sub>2</sub>	12.33	2.02	7.37	5.01	1.71	2.33
CuCl <sub>2</sub>	10.58	1.84	6.45	4.71	1.96	2.07
CuF <sub>2</sub>	8.62	1.63	5.41	3.86	2.26	1.75